

# The saga of neutrinoless double beta decay search with $\text{TeO}_2$ thermal detectors

Chiara Brofferio<sup>1, 2,\*</sup> and Stefano Dell’Oro<sup>3, 4, †</sup>

<sup>1</sup>*Dipartimento di Fisica, Università di Milano-Bicocca, 20126 Milano, Italy*

<sup>2</sup>*INFN, Sezione di Milano-Bicocca, 20126 Milano, Italy*

<sup>3</sup>*Center for Neutrino Physics, Virginia Polytechnic Institute and State University, Blacksburg, VA 24061, USA*

<sup>4</sup>*Gran Sasso Science Institute, 67100 L’Aquila, Italy*

(Dated: January 12, 2018)

Neutrinoless double beta decay ( $0\nu\beta\beta$ ) is a direct probe of physics beyond the Standard Model. Its discovery would demonstrate that the lepton number is not a symmetry of nature and would provide us with unique information on the nature and mass of the neutrinos. Among the experimental techniques employed in the investigation of this rare process, thermal detectors fulfill the requirements for a powerful search, showing an excellent energy resolution and the possibility of scaling to very large masses. In this work, we review the long chain of bolometric experiments based on  $\text{TeO}_2$  crystals that were and continue to be carried out at the Laboratori Nazionali del Gran Sasso (Italy), searching for the  $0\nu\beta\beta$  of  $^{130}\text{Te}$ . We illustrate the progresses and improvements achieved in almost thirty years of measurements and compare the various performance and results. We describe the several steps that led to the CUORE detector, the latest of this series and presently in data taking, and we highlight the challenges that a next bolometric experiment will face in order to further improve the sensitivity, especially concerning the background abatement. Finally, we emphasize the advantages of  $^{130}\text{Te}$  in the search for  $0\nu\beta\beta$  with a further future (and much) expensive experiment.

## CONTENTS

I. Introduction	2	2. CUORE	18
A. $\text{TeO}_2$ bolometers and $0\nu\beta\beta$	2	IV. Limits on the $0\nu\beta\beta$ process	19
II. Bolometric technique	3	A. Constraints on the neutrino masses	21
A. Simplified thermal model	3	V. Challenges for a next bolometric detector	22
B. Phonon sensor	3	A. Improving the sensitivity	22
C. Energy resolution	4	B. Background suppression	23
D. Detector operation	5	1. Contributions to the CUORE	23
1. Response stabilization	5	background	23
E. Properties of $\text{TeO}_2$ bolometers	6	2. Background active rejection	24
III. A long chain of experiments	6	3. CUPID	24
A. Measurements with single crystals	7	VI. Te in the future of the $0\nu\beta\beta$ search	25
1. 6 g crystal	7	VII. Summary	26
2. 21 g crystal	8	Acknowledgments	27
3. 34 g crystal	8	A. Cryogenics apparatus	27
4. 73 g crystal	8	1. DR working principle	27
5. 334 g crystal	8	2. Schematic representation of a DR	28
B. Detector arrays	9	References	29
1. 4 crystal array	9		
2. MiDBD	10		
3. Cuoricino	11		
C. Background studies	13		
1. RAD detectors	13	I. INTRODUCTION	
2. CAW detectors	14		
3. TTT detector	15		
4. CCVRs	16		
D. Towards the tonne-scale	16		
1. CUORE-0	17		

\* chiara.brofferio@mib.infn.it

† sdelloro@vt.edu

Neutrinoless double beta decay ( $0\nu\beta\beta$ ) [1] is a process not predicted by the Standard Model that violates lepton number conservation. The discovery of  $0\nu\beta\beta$  would demonstrate that lepton number is not a symmetry of nature and would establish that neutrinos are Majorana fermions [2, 3]. Furthermore, the study of this process allows us to investigate the nature of the neutrino mass eigenstates.

The huge impact on Particle Physics motivates a strong experimental effort to search for the  $0\nu\beta\beta$  in different isotopes. However, the choice among all the possible  $0\nu\beta\beta$  candidate emitters is narrowed down by the fundamental requests on a high transition Q-value ( $Q_{\beta\beta}$ ) and on the isotopic abundance (i. a.) for either natural or enriched material, as well as on the compatibility with a suitable detection technique. Therefore, the group of “commonly” studied isotopes includes [4, 5]:  $^{48}\text{Ca}$ ,  $^{76}\text{Ge}$ ,  $^{82}\text{Se}$ ,  $^{96}\text{Zr}$ ,  $^{100}\text{Mo}$ ,  $^{116}\text{Cd}$ ,  $^{124}\text{Sn}$ ,  $^{130}\text{Te}$ ,  $^{136}\text{Xe}$  and  $^{150}\text{Nd}$ .

Among these  $0\nu\beta\beta$  candidate emitters,  $^{130}\text{Te}$  is a very favorable one. In fact, this isotope presents important advantages (Table I): the  $Q_{\beta\beta}$  lies between the Compton edge and the full-energy peak of the 2615 keV  $^{208}\text{Tl}$  line, and thus in an acceptable background region for a detector with good energy resolution. This feature, together with the high two-neutrino double beta decay ( $2\nu\beta\beta$ ) half-life, also increases the  $0\nu/2\nu$  event ratio. Moreover,  $^{130}\text{Te}$  i. a., over 30% in natural Te, is the highest among all the isotopes of interest and a further enrichment is a viable option.

Another fundamental characteristic of  $^{130}\text{Te}$  is that this isotope is compatible with more than one detection technique. The first limits on the  $^{130}\text{Te}$  half-life were placed using scintillators [6] and CdTe solid state detectors [7]. However, these detectors are very hard to scale over the kg range, and therefore they are no more competitive. The combination of a tracking device and a calorimeter [8] allowed to set more stringent limits, but also this technique shows a limitation in terms of scalability of the amount of isotope mass. At present, two detector technologies seem to be the most promising choices: metal-loaded liquid scintillator detectors [9] and thermal detectors.

In this work, we will discuss the use of thermal detectors for the search of  $0\nu\beta\beta$  of  $^{130}\text{Te}$ .

### A. $\text{TeO}_2$ bolometers and $0\nu\beta\beta$

The concept of calorimetric detection of energetic particles is very old, since it appears as a pure application of the first law of thermodynamics. In fact, the first example of thermal detection of radiation performed by S. P. Langley dates back to the end of the XIX century<sup>1</sup> [10] and the observation by P. Curie and A. Laborde of radioactive particles via their heat production is only a few years younger [11].

With the birth and evolution of Particle Physics, this idea was also applied to the detection of individual particles. In the late 1940s Andrews and collaborators were able to identify a single particle thanks to a superconducting calorimeter [12]. In fact, it had been earlier suggested by F. Simon that operating these detectors at

TABLE I. Relevant features of  $^{130}\text{Te}$  for the search of  $0\nu\beta\beta$ .

$^{130}\text{Te}$ properties	
$Q_{\beta\beta}$ [keV], [18–20]	$2527.515 \pm 0.013^{\dagger}$
$2\nu\beta\beta$ half-life [ $10^{20}$ yr], [21]	$8.2 \pm 0.2$ (stat.) $\pm 0.6$ (syst.)
i. a. (%), [22]	$34.167 \pm 0.002$
affordability	
$^{\text{nat}}\text{Te}$ [\$/kg], [23]	45
$^{\text{enr}}\text{Te}$ (95% $^{130}\text{Te}$ ) [\$/kg], [24]	20,000

<sup>†</sup> Combined limit from the weighted mean of the individual results in the references.

cryogenic temperatures could significantly improve the sensitivity [13].

However, it was only in the 1980s that new generations of low temperature detectors could be proposed as competitors in several important applications in neutrino physics, nuclear physics and astrophysics [14–17]. Among these, the study of  $0\nu\beta\beta$ .<sup>2</sup>

In particular, the group of E. Fiorini and collaborators began to develop bolometers made of materials containing  $\beta\beta$ -emitters, focusing on the search for the  $0\nu\beta\beta$  of  $^{130}\text{Te}$  using  $\text{TeO}_2$  crystals. The series of measurements performed by this group covers almost thirty years, proving  $\text{TeO}_2$  bolometers to be competitive players in the search for  $0\nu\beta\beta$ .

The first tests on these crystals were performed in the Laboratorio Acceleratori e Superconduttività Applicata of I.N.F.N. (LASA, Segrate (MI), Italy) in 1990. This allowed to perform a series of initial measurements. However, an underground facility represented a fundamental requirement in order to run a rare event physics experiment. The Laboratori Nazionali del Gran Sasso of I.N.F.N. (LNGS [25], Assergi (AQ), Italy, Fig. 1), whose construction had been recently completed at the time, offered a suitable environment for the search for  $0\nu\beta\beta$ .

With their average coverage of about 3600 m. w. e. (meter water equivalent) and the mostly calcareous rock composition [26], LNGS guarantee the very low muon and neutron fluxes of about  $3 \cdot 10^{-8} \text{ cm}^{-2} \text{ s}^{-1}$  [27] and  $4 \cdot 10^{-6} \text{ cm}^{-2} \text{ s}^{-1}$  [28], respectively. Therefore, starting from 1991, these laboratories became the set of a rich activity of experiments and R&D searching for the  $0\nu\beta\beta$  of

<sup>1</sup> Langley calls his new instrument *bolometer* (from the greek  $\betaολή$  +  $\muέτρον$  = ray + meter).

<sup>2</sup> Actually, one should distinguish between radiation and single particle detectors. The word bolometer refers to the former family of devices, the latter being indicated as macro/micro-low-temperature-calorimeters. This separation is especially remarked within the astrophysicist community. However, within the  $0\nu\beta\beta$  community, only macro-low-temperature calorimeters are considered, and these thermal detectors are simply called bolometers. Since this is the custom in the field of  $0\nu\beta\beta$  search, the same choice has been adopted for this work too.

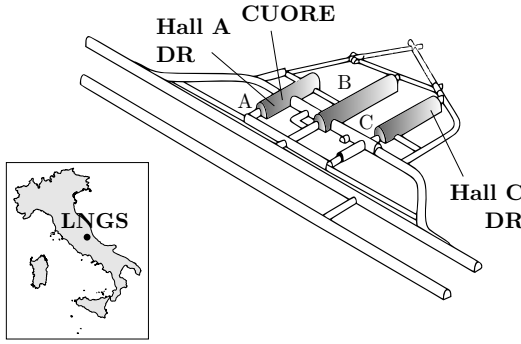


FIG. 1. The LNGS underground laboratories in Italy. The position inside the experimental halls of the infrastructures used for the measurements with  $\text{TeO}_2$  bolometers (see the text for details) is indicated.

$^{130}\text{Te}$  with  $\text{TeO}_2$  bolometers. Since then, many progresses and improvements have been achieved in almost thirty years of measurements and today this technique, that began with crystals of few grams, is now ready for the tonne-scale. The growth in complexity of the subsequent experiments was accompanied by the expansion of the original group. From the initial number of slightly less than ten persons to an international collaborators of about 150 people [29].

## II. BOLOMETRIC TECHNIQUE

Bolometers are calorimeters in which the energy released in the absorber by an interacting particle is converted into phonons and measured via temperature variation. These detectors can be operated only at cryogenic temperatures of about 10 or few tens of mK (see App. A). In fact, the elementary excitation energy is of the order of 10 meV, with a typical corresponding temperature increase of about a few tens/hundreds of  $\mu\text{K}$  per MeV.

Unlike most of the conventional spectroscopic techniques, which are based on the detection of the energy released in the form of ionization and/or excitation of the detector's molecules, the bolometric technique measures the phonon component. This is a great advantage since a considerable fraction, if not all, the released energy is indeed converted into phonon excitations inside the detector. The resulting excellent energy resolution makes these detectors very suitable for the use in rare event physics, such as the search for  $0\nu\beta\beta$ .

### A. Simplified thermal model

A bolometer consists essentially of two elements: an energy absorber, in which the energy from the interacting particle is deposited, and a phonon sensor that converts this energy (i.e. the phonons) into a measurable signal.

In a very simplified model, a bolometer can be represented as a calorimeter with heat capacity  $C$  connected to a heat bath (with constant temperature  $T_0$ ) through a thermal conductance  $G$ . If a certain energy is released in the absorber, this will produce a change in temperature  $\Delta T$  equal to the ratio between  $E$  and  $C$ . Let  $T(t)$  be the absorber temperature as a function of the time  $t$  and let us assume

$$\Delta T \equiv |T(t) - T_0| \ll T_0 \quad \forall t, \quad (1)$$

so that  $C$  and  $G$  can be considered constant quantities. Then, the temperature variation can be described by the time evolution:

$$\Delta T(t) = \frac{E}{C} e^{-t/\tau} \quad \text{where} \quad \tau \equiv \frac{C}{G}. \quad (2)$$

The characteristic time of the thermal pulse is very long, being up the order of few seconds, depending on the values of  $C$  and  $G$ .

From Eq. (2), the crucial importance of the heat capacity appears evident: to get a large signal amplitude,  $C$  has to be as small as possible. In order to minimize  $C$ , very low temperatures are needed and a suitable material for the absorber has to be chosen. In particular, dielectric and diamagnetic crystals or superconductors (below the transition phase) are preferred, so that the main contribution to  $C$  is the one from the crystal lattice. In this case, the Debye law for the specific heat at low temperatures can be applied:

$$C \propto \left( \frac{T}{\Theta_D} \right)^3 \quad (3)$$

where the  $\Theta_D$  is the Debye temperature and is a property of the material. Since this parameter depends on the mass number  $A$  and on the material density  $\rho$  as  $\Theta_D \propto A^{-1/3} \rho^{-1/6}$  [30], low atomic mass and low density should be preferred for their high  $\Theta_D$ . On the other hand, one has to take into account the requirements from particle physics, too. In particular, a high  $Z$  guarantees a larger detection efficiency for  $\gamma$  radiation, while a high  $Z/A$  ratio a larger detection efficiency for  $\beta$ s.

Of course, a real bolometer is much more complicated than the “monolithic” detector here represented. For example, the parameters  $C$  and  $G$  cannot be considered as global quantities, but rather as the sum of many contributions, each with different behaviour. Also the role of the phonon sensor is not negligible in the development of the signal. However, this simple description gives a qualitative idea of a bolometric detector.

### B. Phonon sensor

The phonon sensor is a device that collects the phonons produced in the absorber and generates an electric signal. It is possible to identify many classes of phonon sensors,

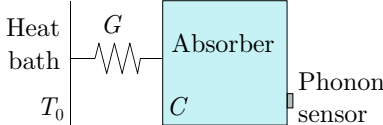


FIG. 2. Simplified bolometer thermal model. The detector is modeled as a single object with heat capacity  $C$  coupled to the heat bath (with constant temperature  $T_0$ ) through the thermal conductance  $G$ . The phonon sensor plays no active role.

sensitive to phonons before or at different phases of the thermal equilibrium (see e.g. Ref. [31] for a review).

A simple version consists in the use of a thermistor whose resistance as a function of temperature has a steep slope, so that to a small variation of temperature a measurable variation of resistance is associated. Since the series of experiments considered in this work used, and currently use, semiconductor thermistors, we focus our attention only on this kind of sensors.

Semiconductor thermistors are glued on the crystal absorbers and are thus intrinsically slow devices. They are mainly sensitive to thermal phonons and act as temperature sensors, giving information about the system in thermal equilibrium.

In general, a semiconductor thermistor consists of a small Ge (or Si) crystal with a doped region. A very uniform and large dopant distribution and a very accurate net dopant concentration are usually obtained through the Neutron Transmutation Doping (NTD) [32]. In this method, the semiconductor sample is bombarded with neutrons which induce nuclear reactions on the various target stable isotopes leading to the formation of n- and p-dopants.

For intrinsic semiconductors (i. e. without impurities) the conduction can happen with an activation energy equal or larger than the energy gap,  $E_{\text{gap}}$ . This mechanism is only possible at high temperatures since the concentration of free charges follows an exponential law with  $T$ :  $n \sim T^{3/2} \exp[-E_{\text{gap}}(T)/(2k_B T)]$ . As an example,  $n \simeq 2.4 \cdot 10^{13} \text{ cm}^{-3}$  for Ge at room temperature but close to zero already at 100 K.

Instead, if impurities are present in the semiconductor lattice, it is possible for the electronic conductance to take place also at lower  $T$ . The mechanisms of “banding” and “hopping” occur in semiconductors which are heavily doped and compensated (equal number of donors and acceptors), respectively. In these cases, the charge carriers move from one impurity to the next without reaching the band.

The banding mechanism requires an impurity concentration high enough to lead to the substantial overlap between neighboring wave functions. The individual impurity states form an “impurity band” [33]. Depending on the number of doped atoms, therefore, the semiconductor can behave either as an insulator or as a metal, even at low  $T$ . In general, it exists a critical concentration  $N_c$  characterizing the (abrupt) transition between

the two opposite situations, which is called the metal-insulator transition (MIT) [34].

The hopping mechanism, instead, occurs when compensating (or minority) impurities create a number of majority impurities which remain ionized down to  $T = 0$  K. In this case, the charge carriers can “hop” from an occupied majority impurity site to an empty one via quantum mechanical tunneling through the potential barrier which separates the two dopant sites. The conduction is activated by phonon mediation. The tunneling probability is exponentially dependent on the inter-impurity distance and this is why an extreme homogeneity of the dopant distribution is fundamental.

In particular, if the dopant concentration is slightly lower than  $N_c$ , then the resistivity is strongly dependent on the temperature. This is why it is usually chosen to operate semiconductor thermistors just below the MIT region. The conduction mechanism in these conditions takes the name of “variable range hopping”, since the carriers can also migrate to far sites if their energy levels are localized around the Fermi energy. The resistivity as a function of the temperature is described by the following law:

$$\rho = \rho_* \exp\left(\frac{T_*}{T}\right)^\gamma \quad (4)$$

where  $\rho_*$  and  $T_*$  are parameters depending on the doping level and compensation. The exponential  $\gamma$  in the Mott model for a 3-dimensional crystal is equal to 1/4 for low compensation values [34]. It becomes 1/2 for large values of compensation, where the Coulomb repulsion among the electrons leads to the formation of a gap in the electron state density near the Fermi energy [35].

### C. Energy resolution

The intrinsic energy resolution of a detector is primarily determined by the statistical fluctuation of the number of elementary events contributing to the signal. In fact, for a given energy deposition in the detector, more channels for the energy transfer are available, while usually only one (e. g. scintillation or ionization) can be used in the detection.

In the case of a sensor sensitive to thermal phonons, instead, one expects no fluctuation on the production of energy carriers, since all the released energy is sooner or later converted into phonon excitations. The effective number of phonon modes in the detector at thermal equilibrium is  $N = C(T)/k_B$ , each with quantum occupation number 1, RMS fluctuation of 1 phonon and mean energy  $\varepsilon = k_B T$  [17]. As an example, for a 750 g TeO<sub>2</sub> crystal at 10 mK ( $C \simeq 2.2 \text{ nJ K}^{-1}$  [36]), this gives  $N \simeq 1.6 \cdot 10^{14}$ .

The number of these elementary events follows a Poisson distribution with  $\Delta N = \sqrt{N}$  due to the continuous phonon exchange between the absorber and the heat sink. Therefore, the intrinsic energy resolution  $\Delta E$  is propor-

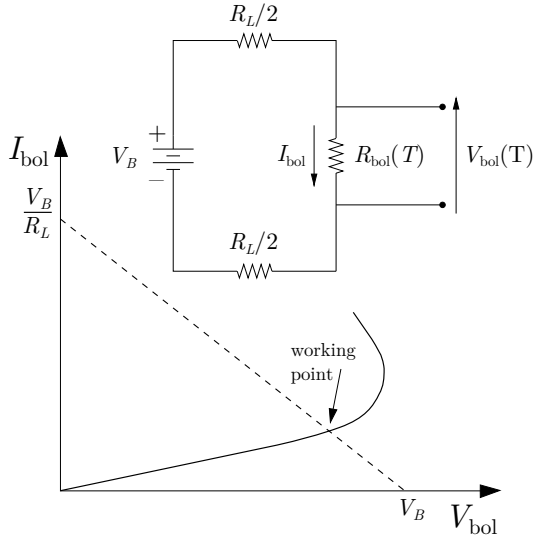


FIG. 3. (Top) Electric scheme of the biasing system used for the NTD readout. (Bottom) Typical load curve of a semiconductor thermistor. The working point is set as the intersection between the  $V$ - $I$  characteristic curve and the load line  $V_{\text{bol}} = V_B - I_{\text{bol}} R_L$ .

tional to the mean energy of the elementary excitation:

$$\Delta E \propto \varepsilon \Delta N = \xi \sqrt{k_B C(T) T^2}. \quad (5)$$

The factor  $\xi$  is a dimensionless factor that depends on the details of the real detector. It can be made of the order of unity with a proper optimization work [17]. It is worth to notice that the expression obtained in Eq. (5) is *independent* of energy. To give an idea of the potentiality of these detectors, the intrinsic resolution for the considered 750 g TeO<sub>2</sub> crystal lays within the range (20 – 100) eV.

However, most of the time the effective energy resolution of these kind of detectors is dominated by the “extrinsic” noise generated by a variety of uncorrelated sources that are almost impossible to cancel completely [37, 38]. These include Johnson noise, thermal noise (i.e. noise temperature instabilities of the heat sink), noise from the electronics readout and the cryogenic system, mechanical vibrations, … Eventually, the combination of the multiple factors often results in an energy resolution of the order of a few keV at 1 MeV (see Sec. III), a value anyhow comparable with that of the best performing detectors.

#### D. Detector operation

In order to obtain a voltage signal, a steady current  $I_{\text{bol}} = I_B$  (bias current) is sent through the thermistor by means of the bias circuit shown in Fig. 3. The voltage generator is closed on a load resistor  $R_L$  in series with the thermistor  $R_{\text{bol}}$ , whose resistance is negligible in comparison to  $R_L$  ( $R_L \gg R_{\text{bol}}$  therefore  $I_{\text{bol}}$  is independent from  $R_{\text{bol}}$ ).

Once a working point is set by forcing a bias current (Fig. 3), a voltage drop  $V_{\text{bol}}(T) = I_B R_{\text{bol}}(T)$  is established across the thermistor. The consequent power dissipation  $P = I_B V_{\text{bol}}$  produces a temperature rise and acts back on the resistance  $R_{\text{bol}}(T)$  until an equilibrium is reached:

$$T_{\text{bol}} = T_0 + \frac{P}{G} \quad (6)$$

where  $G$  the thermal conductance between the detector and the heat sink ( $T_0$ ).

This phenomenon makes the  $V$ - $I$  relation deviate from linearity and leads to a non-ohmic behavior. It is often referred to as “electrothermal feedback”. For a given  $I_B$ , the “static” resistance is simply the ratio  $V_{\text{bol}}/I_{\text{bol}}$  while the “dynamic” resistance is the inverse of the tangent to the  $V$ - $I$  curve. By further increasing  $I_B$ , the dynamic resistance crosses the so called “inversion point” (where it vanishes) and becomes negative. The intersection of the  $V$ - $I$  curve, usually called *load curve*, with the load line imposed by the biasing system determines the working point of the sensor (Fig. 3). This is typically chosen before the inversion point in order to maximize the signal amplitude and the signal-to-noise ratio. By a combined fit of load curves measured at different base temperatures, it is possible to evaluate the thermistor intrinsic parameters  $\rho_*$ ,  $T_*$  and  $\gamma$ .

In first approximation, the thermal pulse produced by an energy release in the absorber is characterized by a very fast rise time (instantaneous if we assume the model described in Sec. II A and a negligible thermalization time). The fall time, instead, follows an exponential decay whose time constant depends on the physical characteristic of the detector (recall Eq. (2)). The relationship between the electrical pulse height  $\Delta V_{\text{bol}}$  and the energy deposition  $E$  can be obtained by resolving the circuit of Fig. 3:

$$\Delta V_{\text{bol}} = \text{const} \cdot \gamma \left( \frac{T_*}{T_{\text{bol}}} \right)^\gamma \cdot \frac{E}{C \cdot T_{\text{bol}}} \cdot \sqrt{P \cdot R_{\text{bol}}} \quad (7)$$

where  $P$  is the power dissipated in the thermistor  $R_{\text{bol}}$  by Joule effect. In particular, this expression vanishes in the limits  $P \rightarrow \infty$  and  $C \rightarrow \infty$ .

To make an example, an energy deposition of 1 MeV in a 750 g TeO<sub>2</sub> absorber at 10 mK (see Sec. II E) typically produces a temperature increase  $\Delta T \sim 100 \mu\text{K}$ , with a related voltage drop  $\Delta V_{\text{bol}} \sim 100 \mu\text{V}$ .

#### 1. Response stabilization

A critical issue when operating bolometric detectors over long periods of time, for months or even for years, consists in maintaining a stable response, despite the unavoidable temperature fluctuations due to the cryogenic setup.

An effective approach to this issue can be found in the use of a pulser able to periodically deliver a fixed (and

extremely precise) amount of energy to the detector and to generate a pulse as similar as possible to the signal corresponding to a real event [39, 40]. In this way, the study of the variation of the detector response to the same energy deposition can be used to correct (off-line) the effects of the cryogenic instabilities.

A particle-based stabilization would present the advantage of getting an identical detector response to the pulser and to the events of interest. However, this method would present some important drawbacks: a series of undesired cascade peaks would be generated by the same source and the Poisson time distribution of the events would limit the calibration rate. Furthermore, the calibration pulses could not be “flagged” and their off-line identification would be based only on their amplitude.

Instead, a resistive element thermally coupled to the crystal, can be used to inject calibrated amounts of energy via Joule heating. This solution offers the advantage of a complete control of the calibration mechanism: the pulses can be equally spaced in time and their rate and amplitudes can be easily tuned to the necessity of the experiment. Anyhow, it has to be noted that such a heating element needs to satisfy some (non-obvious) requirements. In particular, its resistance must be reasonably independent of the temperature and of the applied voltage, while its heat capacity must be negligible with respect to the detector’s one. In order to provide an almost instantaneous energy release, the relaxation time to the crystal of the developed heat must be much shorter than all the typical thermal time constants. Finally, the mechanism of signal formation for particle interactions and for Joule heating must be similar enough to assure that the pulse amplitude dependence on time, baseline level and other operation conditions are the same for the two processes.

Steady resistances useful for this purpose can be realized through a heavily doped semiconductor, well above the MIT region, so that a low-mobility metallic behaviour is exhibited [41]. In particular, silicon heaters have been used for the detector response stabilization in the experiments described in Sec. III.

### E. Properties of $\text{TeO}_2$ bolometers

Tellurium dioxide,  $\text{TeO}_2$ , is a particularly suitable material to be employed in cryogenic particle detectors.  $\text{TeO}_2$  is the most stable oxide of Te [42] and presents favorable thermodynamic characteristics.  $\text{TeO}_2$  crystals are both dielectric and diamagnetic with a relatively high value of the Debye temperature ( $\Theta_D = (232 \pm 7)$  K [36]). The very low heat capacity at cryogenic temperatures leads in turn to large temperature variations from tiny energy releases, which is at the base for a high energy resolution bolometer. Moreover, the fact that the thermal expansion of  $\text{TeO}_2$  crystals is very close to that of copper [43, 44], allows the use of this metal for the detector mechanical support structure without placing too

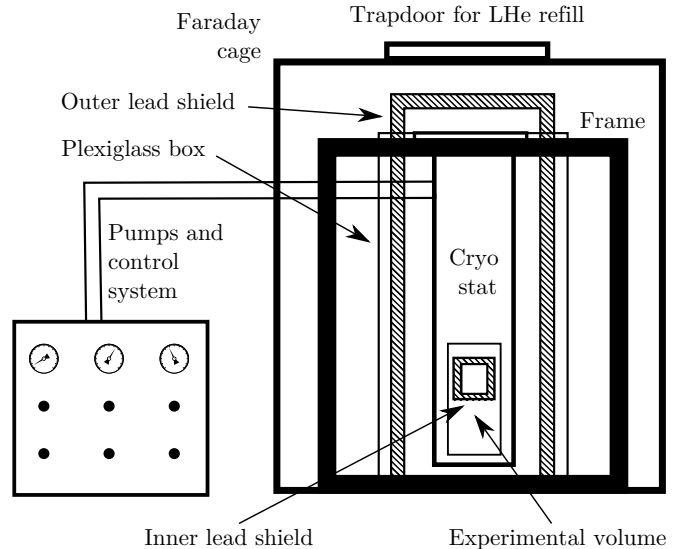


FIG. 4. Schematic of the cryogenic system in the Hall A of the Laboratori Nazionali del Gran Sasso. Figure from Ref. [52].

much strain on the crystals during the system cool down.

$\text{TeO}_2$  is present in nature in two mineral forms: orthorhombic tellurite ( $\beta\text{-TeO}_2$ ) and paratellurite ( $\alpha\text{-TeO}_2$ ). In particular, paratellurite, is commercially produced at the industrial scale. In fact, thanks to its acoustic and optical properties (paratellurite is a colorless tetragonal form of  $\text{TeO}_2$ ), this compound is in fact employed in ultrasonic light deflectors and in laser light modulators [45]. These crystals have mechanical and optical characteristics fully compliant with the requirements for the use as thermal detectors. Moreover, the numerous improvements in preparing the  $\text{TeO}_2$  powder and in growing the crystals allow the production of almost perfect large specimens (bubble-free, crack-free and twin-free) from which it is possible to construct bolometers with masses of the order of  $\sim 750\text{ g}$  [46, 47] or more [48, 49].

It is fundamental to notice that the use of a material inside a  $0\nu\beta\beta$  detector imposes very stringent constraints in terms of radiopurity. Therefore, tight limits must be set for the crystal impurity content in order to get an acceptable background rate.  $\text{TeO}_2$  also satisfies these requirements. Thanks to dedicated production lines for the raw powder synthesis, the crystal growth and the surface processing, crystals with bulk contaminations of the order of  $\lesssim 10^{-13}\text{ g/g}$  for  $^{238}\text{U}$  and  $^{232}\text{Th}$  are available [47, 50]. At the same time, dedicated surface treatments translate in surface contamination levels of a few  $10^{-9}\text{ Bq cm}^{-2}$  for both  $^{238}\text{U}$  and  $^{232}\text{Th}$  [50, 51].

## III. A LONG CHAIN OF EXPERIMENTS

Early measurements of  $\gamma$ -ray spectroscopy with bolometers were carried out at LASA, where a Dilution

Refrigerator (DR, see Sec. A) from Oxford Instruments was installed in 1987 [53]. Initially, pure Te crystals (2.1 g [54] and 28 g [55]) were tested, but the metal was found to be too brittle at low temperatures. A positive outcome was instead obtained by the use of  $\text{TeO}_2$  crystals (6 g [56] and 21 g [57]). Given the promising results, the same crystals were operated also at LNGS.

A DR (also by Oxford Instruments) was installed in the Hall A of LNGS in 1989 [58] (Fig. 1). A schematic of the cryogenic system is shown in Fig. 4.<sup>3</sup> The detector was contained in an Oxygen Free High Conductivity (OFHC) copper frame. The DR was constructed with specially chosen low radioactivity components. All materials inside the refrigerator had been previously tested for radioactivity with a germanium spectrometer. The system was built in order to load tens of kg at low temperature, so that it would have become possible to install radioactive shields inside the cryostat and run large bolometric arrays. Indeed, starting after the first few runs, different lead shields were added and changed depending on the geometry of the current detector. Outside the DR, a 10 cm minimum thickness lead layer protected the system against external radioactivity. Later, another 10 cm layer made of low radioactivity lead was added (internally to the previous one) and the shield was enclosed in a Plexiglas box with anti-radon purpose, constantly flushed with nitrogen gas from a  $\text{LN}_2$  evaporator. The cryogenic system, together with the readout electronics, were in turn contained inside a Faraday cage in order to minimize electromagnetic interferences.

This low-radioactivity cryogenic infrastructure, inside an underground site, represented the ideal facility for the study of rare events, such as  $0\nu\beta\beta$ .

### A. Measurements with single crystals

Given the favorable environment offered by the Hall A DR, in order to perform an experimental search for  $0\nu\beta\beta$ , it was now crucial to construct a suitable low-background bolometric detector. In particular, a critical point consisted in the design of crystal holder, since this element would have strongly affected both the detector performance and the background rate.

The holder had to provide mechanical support and to steady keep the detector in place (to hold indeed) while, at the same time, it had not to constitute a (strong) thermal link to the heat sink. In this way, the heat would have been conducted away from the absorber only via the thermistor (and hence measured) and the crystal would have been prevented to oscillate around its equilibrium position, due to the vibrations induced by the refriger-

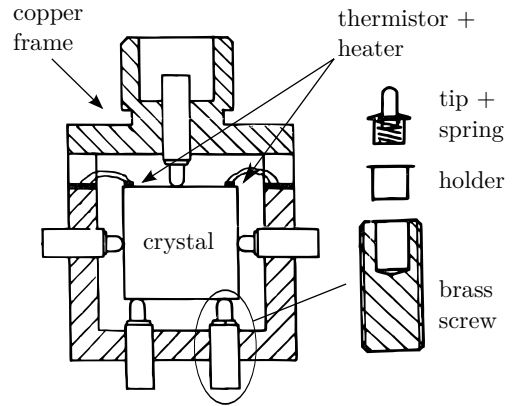


FIG. 5. Cross section of the frame used to hold the 6 g, 21 g and 34 g crystal bolometers. Figure from Ref. [56].

ator cooling unit.<sup>4</sup> A compromise between a good mechanical support and a weak thermal contact had to be found in order to minimize the effects of the loss in the signal amplitude and to prevent the generation of microphonic noise. Moving in this direction, the crystal was suspended with brass screws whose extremities had small spring loaded needles which could exert an adjustable pressure (Fig. 5).

Therefore, the first measurements performed at LNGS had also the goal of investigating the background level of the whole experimental apparatus and of testing the effectiveness of the adopted solutions.

#### 1. 6 g crystal

The 6 g crystal [56] was operated in two following runs of 370 h and 260 h, respectively. The first run presented an excessively high  $\alpha$  counting, with the  $^{210}\text{Po}$  peak clearly visible in the background spectrum (light spectrum in Fig. 6). The source of the contamination was identified in the tin used for the soldering required to fix the needles, which was directly facing the detector, to the screws. Once the tin was eliminated (dark spectrum in Fig. 6), the average background rate in the (3 – 11) MeV interval passed from  $(2.92 \pm 0.09)$  counts  $\text{h}^{-1}$  to  $(0.6 \pm 0.05)$  counts  $\text{h}^{-1}$ . In the Region of Interest (ROI) around the  $^{130}\text{Te}$   $Q_{\beta\beta}$ , the measured value was  $8 \cdot 10^{-5}$  counts  $\text{keV}^{-1} \text{h}^{-1}$ . The achieved energy resolution was  $\sim 50$  keV FWHM, rather independent of the energy.

The 6 g crystal allowed to set the first, already competitive, limit on the  $^{130}\text{Te}$   $0\nu\beta\beta$  half-life with a  $\text{TeO}_2$

<sup>3</sup> The setup actually evolved over the years, as it will become clear from the following sections.

<sup>4</sup> Vibrations cause an increase of the operating temperature since they dissipate power by means of mechanical friction, in turn increasing the detector heat capacity (recall Eq. (2)). This mechanism generates noise due to the random vibrational heating and microphonic noise due to the modification of the parasitic electrical capacitance shunting the current across the thermistor.

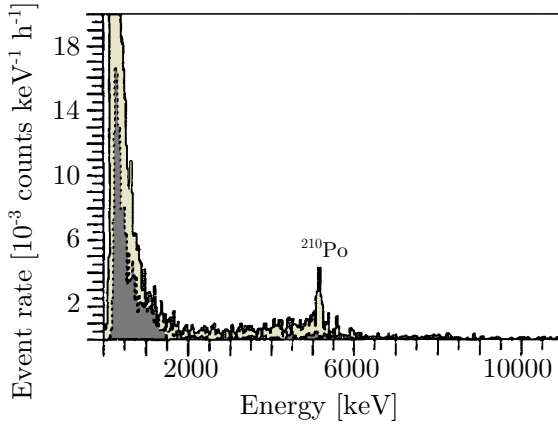


FIG. 6. Background spectra of the 6 g  $\text{TeO}_2$  bolometric detector acquired during the first (light) and second (dark) runs. The contribution to the  $\alpha$  background coming from the solderer is clearly visible in the former spectrum. Figure from Ref. [56].

bolometer (see Sec. IV). This was one of the first physics results ever obtained with the bolometric technique.

#### 2. 21 g crystal

The 21 g crystal [57] was operated for  $\sim 160$  h, keeping the same configuration for the detector holder (Fig. 5). Anyway, the new crystal exhibited a FWHM energy resolution of  $\sim 20$  keV at 2615 keV, which represented an improvement of more than a factor 2. This was obtained thanks to a better thermistor and an optimized mounting using new spring loaded tips. The main limitations to the resolution remained the microphonic and the electronic noise and the instabilities in the operating temperature. At the same time, the careful selection of the material facing the detector and a proper choice of the crystal itself allowed to keep the background in the ROI, mainly due to  $\alpha$  contamination, at the level of  $10^{-2}$  counts  $\text{keV}^{-1} \text{kg}^{-1} \text{h}^{-1}$ .

#### 3. 34 g crystal

A 34 g crystal [59] was operated shortly after the 21 g one in the usual setup. The live time of the experiment was over 1050 h, thus obtaining a  $\sim 10$  times larger exposure (i.e. with the product detector mass times live-time, see Sec. IV for details). The background level was compatible with the one obtained in the previous run. The energy resolution worsened instead of a factor 2 ( $\sim 40$  keV above 1 MeV). In fact, in order to check a possible background contribution coming from the heater resistor (see Sec. IID 1), the chip was not glued on the crystal. A  $^{60}\text{Co}$  and a  $^{232}\text{Th}$  sources illuminating the detector (through a small window in the lead shield that

could be opened) were thus used to check the detector response stability, which remained lower than 1% over the initial  $\sim 440$  h of operation [60]. However, the absence of a response stabilization system reflected into some non linearities in the spectrum (Fig. 7). In the end, the hypothesis on a significant contribution to the background coming from the heater itself was found to be wrong.

#### 4. 73 g crystal

The next measurement was carried out with a 73 g crystal [63]. This time, an improved version for the crystal holder was used (Fig. 8). The detector was operated for more than four months in two following runs of 1389 and 1046 hours of effective live-time, respectively. In between, an inner ultra-low activity lead shield of 3.5 cm minimum thickness was inserted inside the cryostat (Fig. 4). This was completely surrounding the detector and allowed to reduce the background of a factor  $\sim 2$  in the ROI (around 2.5 MeV), bringing it to less than one quarter with respect to that of the 34 g crystal. The strong background suppression is clearly visible in the comparison between the spectra acquired in the two runs, as shown in Fig. 9. The obtained energy resolution was extremely good: 7 keV FWHM in the ROI, not too different from that of a Ge diode.

#### 5. 334 g crystal

The successive measurement represented an important breakthrough for the bolometric technique. The new detector, a  $3 \times 3 \times 6$  cm $^3$  crystal of 334 g [64], was indeed the largest thermal detector operated so far. Although the resolution was worse than that of the 73 g crystal, still

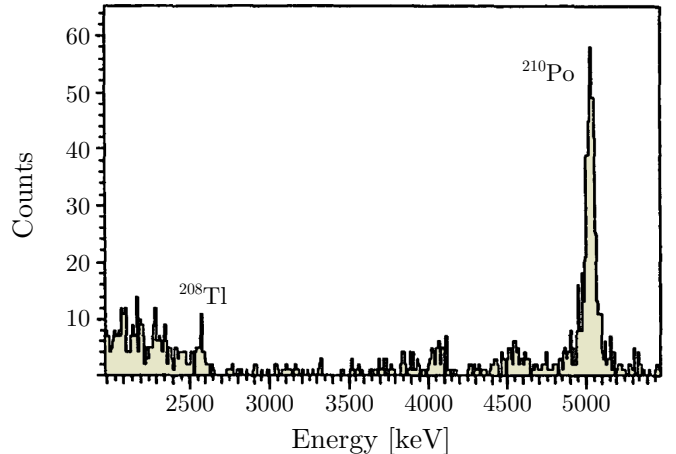


FIG. 7. Background spectrum of the 34 g  $\text{TeO}_2$  bolometric detector obtained in 1051.4 h. It is possible to observe non linearities effects (enlargement of the peaks at higher energies) due to the absence of stabilization heater. Figure from Ref. [59].

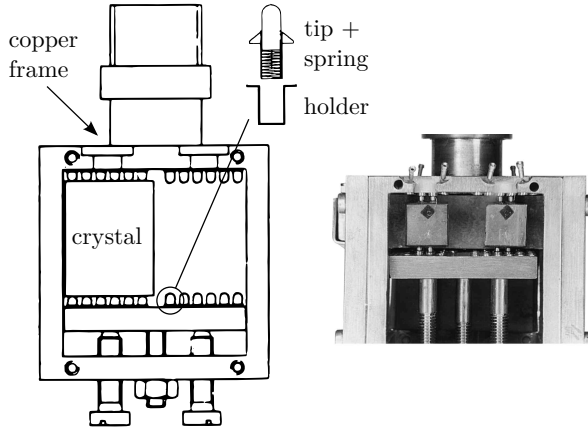


FIG. 8. (Left) Cross section of the frame used to hold the 73 g and 334 g crystal bolometers. Figure from Ref. [61]. (Right) The same frame during the radioactivity measurements of the Roman lead used for the DR internal shielding. Figure from Ref. [62].

mainly limited by the microphonic and electronic noise, it remained similar to the ones previously obtained. On the contrary, the background in the ROI was reduced to about  $4 \cdot 10^{-4}$  counts  $\text{keV}^{-1} \text{kg}^{-1} \text{h}^{-1}$ . In total, more than 10500 h of effective running time [65] were collected in about 18 months. This translated into a factor 50 of increase in the exposure.

### B. Detector arrays

During the period of the 334 g crystal run (around 1994), the growth technique for  $\text{TeO}_2$  did not allow to produce specimens with mass larger than  $\sim 0.5 \text{ kg}$  without risks of defects and fragility [66]. Therefore, in order to improve the sensitivity by further increasing the exposure, it became necessary to begin to assemble arrays of bolometers.

With the growth in complexity of the detectors and, especially, due to the very long data taking periods in the Hall A DR, the use of a dedicated test facility became fundamental in view of the new generation of experiments [67]. In 1992, a new DR was installed inside the Hall C (Fig. 1). Similarly to the one in Hall A, the Hall C DR was built with low radioactive materials and, over the years, provided with an external shielding in all directions (15 cm lead + copper) and an anti-radon Plexiglas box. The internal shielding (against the contamination from the dilution unit materials) was provided by a 5.5 cm lead layer just above the detector. This was made of ancient Roman lead (I century b.C., Hispanic origin) with a  $^{210}\text{Po}$  activity less than  $4 \text{ mBq kg}^{-1}$  [62]. Inside the cryostat, a new system of mechanical suspensions was implemented to reduce vibration and thermal noise [68, 69].

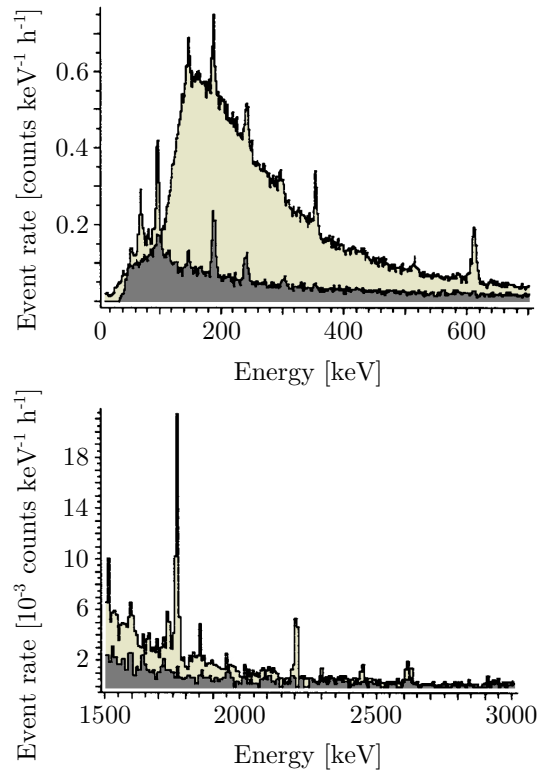


FIG. 9. Background spectra of the 73 g  $\text{TeO}_2$  bolometric detector acquired during Run I (light) and Run II (dark). The effect of the new lead shield on the background is clearly visible. (Top) (0 – 700) keV energy region (Bottom) (1500 – 3000) keV energy region. Figure from Ref. [63].

#### 1. 4 crystal array

The first array of  $\text{TeO}_2$  bolometers was constituted by 4 crystals very similar both in mass and in dimensions to the last operated one [67]. The levels of the crystal internal contamination were satisfactory:  $4 \cdot 10^{-13} \text{ g/g}$  for  $^{238}\text{U}$  and  $1.2 \cdot 10^{-12} \text{ g/g}$  for  $^{232}\text{Th}$ . A new concept for the crystal holder was adopted and tested in the Hall C DR in 1994. The spring loaded tip system was substituted with PTFE frames, which allowed to reduce the radioactive contamination (Fig. 10).

A physics run with the new detector was then performed in the Hall A cryostat [70]. The 4 crystal array constituted the first bolometric  $0\nu\beta\beta$  experiment with over 1 kg of mass. Unfortunately, one thermistor over 4 turned out to be damaged. In 1995,  $\sim 4$  months of active live-time could be collected [66]. The installation of a reliquefier (directly connected to the DR) required quite a time to reassess the system, decreasing the duty cycle of the experiment.<sup>5</sup> The final exposure was therefore lower than that obtained with the 334 g crystal alone. Anyway,

<sup>5</sup> This system avoided the need of frequent LHe refills and guaranteed a constant LHe level, thus stabilizing the internal temper-

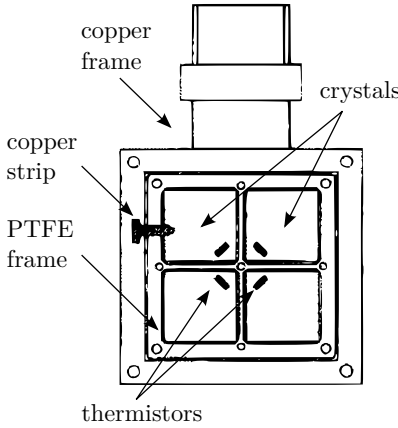


FIG. 10. Cross section of the frame used to hold the 4 crystal array. Figure from Ref. [67].

this measurement proved that the same good conditions of resolution and background rate were achievable even with a complex system of bolometers. The 4 crystal array represented a prototype for a more complex detector to come.

## 2. MiDBD

In the late summer of 1997, a tower made of 20 bolometers (5 floors of 4 crystal each) was assembled and installed inside the Hall A DR [73]. This experiment was later named MiDBD (Milan Double Beta Decay). The single module absorber consisted of a “standard”  $3 \times 3 \times 6 \text{ cm}^3$  crystal, for a total  $\text{TeO}_2$  mass of about 6.8 kg. In particular, since March 1999, four natural crystals were replaced with four isotopically enriched crystals, two  $^{128}\text{Te}$  (82.3%) and two in  $^{130}\text{Te}$  (75.0%).<sup>6</sup> MiDBD was thus the new largest operating cryogenic mass.

The tower frame was made of OFHC copper, in turn connected via an OFHC copper cold finger to the MC. As for the 4 crystal array, the individual bolometers were fastened to this structure by means of PTFE and copper supports (left side in Fig. 11). The detector was laterally surrounded by a 1 cm Roman lead shield and enclosed between two 10 cm thick disks, also made of Roman lead.<sup>7</sup>

A new dedicated front-end system for the readout of the large array was developed, which allowed to remotely set all the necessary parameters for each detector [74, 75].

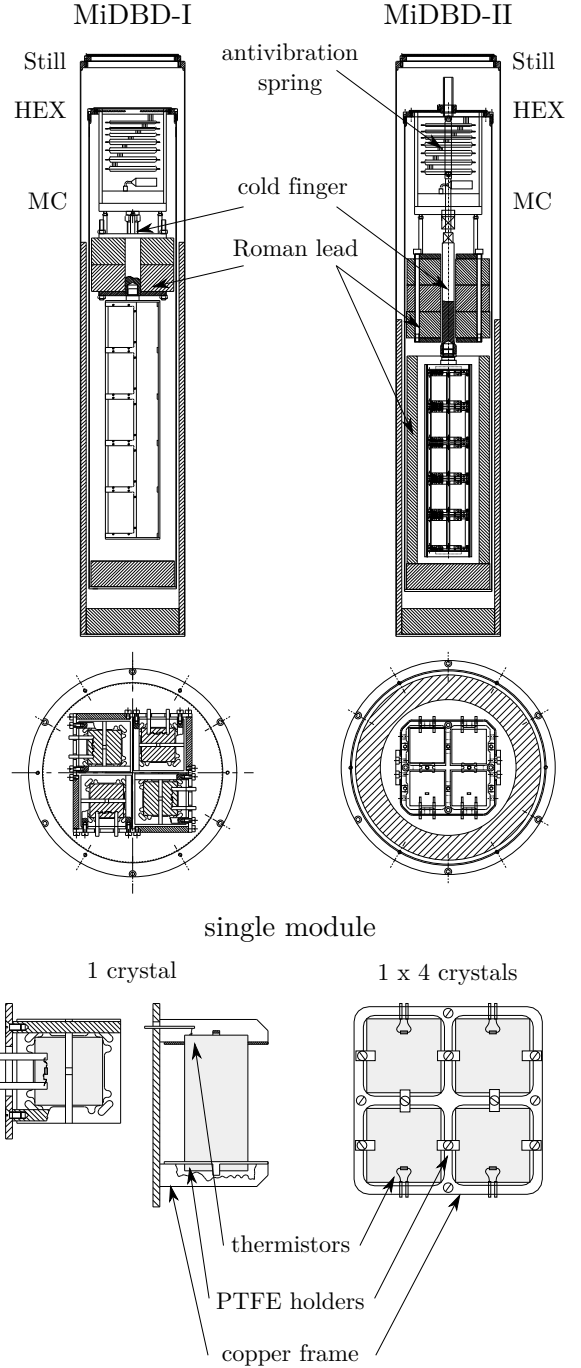


FIG. 11. Schematic of the MiDBD experiment: comparison between the old and the new configuration with a detailed view of the single modules. Adapted from Refs. [71, 72].

atures of the DR. It will be used until September 2004, during the run of Cuoricino (see Sec. III B 3), and then abandoned due to its complexity. In fact, the liquefier required very frequent maintenance, thus reducing the live-time of the experiment.

<sup>6</sup> The enriched crystals allowed to study the  $2\nu\beta\beta$  by analyzing the different spectra [71].

<sup>7</sup> In particular, the detector had to be protected from the intrinsic radioactive contamination of the dilution unit materials (e.g. from silver and stainless steel).

In a preliminary run, intended to test the overall performance of the array, only a part of the readout electronics was ready. As a consequence only eight channels could be read out simultaneously [76]. Then, the system became fully operative and data for a total of 31508 kg h of exposure were collected (MiDBD-I). The major improvement with respect to the previous measurement consisted in the drastic (almost a factor 10)

suppression of the background rate, now at the level of  $(0.59 \pm 0.06)$  counts  $\text{keV}^{-1} \text{kg}^{-1} \text{yr}^{-1}$ . Still, a further reduction would have allowed to fully exploit the potentiality of the new detector, and in turn to significantly improve the sensitivity on the  $0\nu\beta\beta$  search. The results from MiDBD-I also showed that, to gain in terms of overall detector performance, it was necessary to reduce the spread among the single bolometer performance.

At the beginning of 2001, the MiDBD detector was therefore completely dismounted and remounted in a new configuration [71]. A comparison between the old and the new configurations is shown in Fig. 11 (see also Fig. 13): it can be seen that the differences between MiDBD-I and MiDBD-II were very significant. A more compact assembly of the crystals was adopted. The fundamental module was not anymore constituted by a single crystal, but by each plane of the tower (bottom panel in the figure). On the one side, the new design allowed to perform a better anti-coincidence analysis. On the other, it allowed to reinforce the Roman lead shield. The thickness of the lead layer between the MC and the detector was increased by 5 cm and a new lateral shield of 2 cm minimum thickness was added. Moreover, the PTFE masks were substituted

by small PTFE pieces, with a consequent reduction of the material facing the crystals. New electric connections with copper pins avoided the use of the soldering indium (rich in the contaminant  $^{115}\text{In}$ ), since the gold wires from the thermistors could now be crimped to the pins and an anti-vibration damping method was implemented to reduce mechanical noise. Finally, both the crystals and the copper were cleaned in order to reduce their own radioactive contamination and that coming from the production process.

The detector was operated in the new configuration for almost a year (5690 kg h of exposure). The individual FWHM energy resolutions at the 2615 keV line ranged from 5 to 15 keV. As shown in the spectra of Fig. 12, the introduced changes translated in a clear reduction both in the continuum and in the peak intensities with respect to MiDBD-I: a factor  $\sim 2$  for the  $^{238}\text{U}$  and  $^{232}\text{Th}$   $\alpha/\gamma$  peaks and for the (3–4) MeV continuum and a factor 4 for the 5.3 and 5.4 MeV peaks of  $^{210}\text{Po}$ . A reduction of a factor  $\sim 1.5$  was observed in the gamma continuum between 1 and 3 MeV, with the background level in the  $0\nu\beta\beta$  energy region of  $(0.33 \pm 0.11)$  counts  $\text{keV}^{-1} \text{kg}^{-1} \text{yr}^{-1}$  (see the discussion on the background in Sec. III C).

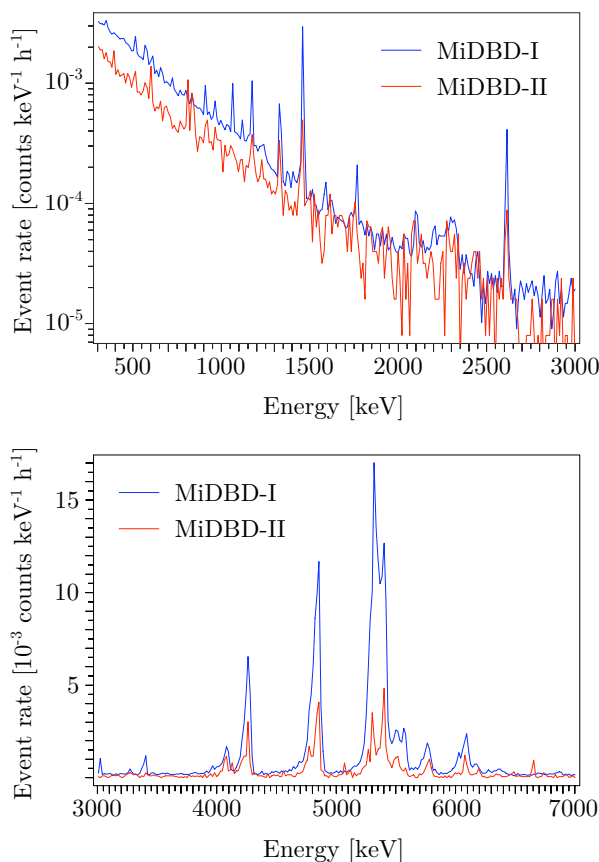


FIG. 12. Background comparison between MiDBD-I (blue) and MiDBD-II (red). (Top) (300 – 3000) keV energy region (Bottom) (3000 – 7000) keV energy region. Figure from Ref. [77].

### 3. Cuoricino

Already during the early preparation phase of the MiDBD experiment (summer 1997), a very ambitious project was proposed by Fiorini and collaborators, i.e. to build “an array of 1000 cryogenic detectors of a mass between 0.5 and 1 kg each” [80]. The main goal remained the search for  $0\nu\beta\beta$ , but this experiment would have allowed also studies on the interaction of WIMPS and solar axions and on rare decays. The name chosen for the new detector was CUORE, acronym for Cryogenic Underground Observatory for Rare Events (Italian for ‘heart’). The realization of such a complex cryogenic setup would have required the support of a numerous (international) collaboration and many years of preparation. As a first step towards CUORE, a simpler (and much less expensive) experiment was also proposed. The original idea foresaw an array made of 100  $5 \times 5 \times 5 \text{ cm}^3$  crystals for a total mass of about 75 kg, hence the name Cuoricino (Italian for “small CUORE”). Cuoricino had not to be purely considered a proof of concept for CUORE, but an independent experiment as well. In fact, apart from becoming by far the new largest cryogenic detector, Cuoricino would have contained about 20 kg of  $^{130}\text{Te}$ , a mass three times larger than the whole MiDBD and, more in general, larger than the  $\beta\beta$ -isotope mass of any other  $0\nu\beta\beta$  experiment running at the time.

Once Cuoricino was approved, a first  $5 \times 5 \times 5 \text{ cm}^3$  760 g  $\text{TeO}_2$  crystal was operated as a bolometer for  $\alpha$ - and  $\gamma$ -ray spectroscopy in the Hall C DR [81].<sup>8</sup> The

<sup>8</sup> The larger size was obtained after changing the direction of



FIG. 13. From left to right: the MiDBD-II, Cuoricino and CUORE-0 towers in relative scale. (Top) The completed towers. (Bottom) The towers attached to the Hall A DR. Adapted from Refs. [72, 78, 79].

achieved FWHM resolution was comparable with that of a Ge detector for high-energy  $\gamma$  and the value of 4.2 keV at the 5407 keV-line of  $^{210}\text{Po}$  was the best ever obtained with any type of detector. The fundamental brick for the construction of the tower was therefore available.

In its final configuration, Cuoricino consisted of 44  $5 \times 5 \times 5\text{ cm}^3$  cubic crystals of  $\sim 790\text{ g}$  mass and 18  $3 \times 3 \times 6\text{ cm}^3$  crystals coming from MiDBD (including the 4 enriched ones). These were disposed in 13 floors, 11 4-crystal modules housing the large crystals and 2 9-crystal modules housing the small ones (Fig. 13). The total mass of  $\text{TeO}_2$  was 40.7 kg. It was resized with respect to the proposed one, but still large enough to make Cuoricino a competitive experiment for the  $0\nu\beta\beta$  search.

A strict protocol was adopted in order to guarantee the radio-purity of the detector. All the crystals were grown with pre-tested low radioactivity material by the Shanghai Institute of Ceramics - Chinese Academy of Sciences (SICCAS, China) and shipped to Italy by sea to minimize the activation by cosmic rays. These were then lapped with specially selected low-contamination polishing compound. All the operations, including the assembly of the tower, were carried out in a clean room environment inside sealed glove boxes constantly flushed with  $\text{N}_2$ .

Significant improvements interested the whole data production chain, with the implementation of a PID controller for the temperature stabilization [82], a new front-end electronics [83] and a software trigger for the data acquisition [84].<sup>9</sup>

Cuoricino [85] took the place of MiDBD in the Hall A cryostat. The cool down occurred at the beginning of 2003 and the start of the data taking shortly after (Run I). In November 2003 the tower was warmed up to perform maintenance operations and to recover some lost connections. The data taking restarted in May 2004 (Run II) and lasted until June 2008, with 50/52 channels now operational. The total collected exposure was 19.75 kg yr of  $^{130}\text{Te}$ .

The best performance, both in terms of background counts and resolution, were reached with the 5 cm-side bolometers. The harmonic mean FWHM weighted on the physics exposure at the  $^{208}\text{Tl}$  line was  $(5.8 \pm 2.1)$  keV at the  $^{208}\text{Tl}$  line [78] (Fig. 22). Regarding the background, the flat continuum in the ROI relative to Run-II was  $(0.153 \pm 0.006)$  for the large crystals and  $(0.17 \pm 0.02)$  counts  $\text{keV}^{-1} \text{kg}^{-1} \text{yr}^{-1}$  for the small crystals, respectively (anyway compatible).

Cuoricino demonstrated the feasibility of running a very massive and complex bolometric detector array for almost five years with the best performance obtained so far. However, although very good, the results in terms of resolution and, especially, of background rate were not

growth of the crystal from  $\langle 100 \rangle$  (that of the MiDBD and previous detector crystals) to  $\langle 110 \rangle$ .

<sup>9</sup> The software trigger was actually introduced in Run-II (see further in text).

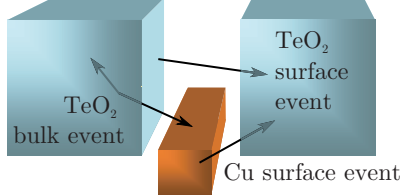


FIG. 14. Sketch of events in which the energy release is only partially deposited in one crystal. Degraded  $\alpha$  particles due to surface contamination of the crystals or of the closest inert material (copper and PTFE) represent a dangerous background for the  $0\nu\beta\beta$  search.

yet compliant with the tight limits set for the CUORE detector.

### C. Background studies

With MiDBD, a systematic study of the radioactive contaminations dangerous for the  $0\nu\beta\beta$  search was started. A background model able to describe the observed spectra in terms of contaminations from the materials directly facing the detector, the whole cryogenic setup and the environmental radioactivity was developed and supported by detailed Monte Carlo simulations of the detector geometry [77]. This model allowed to account for the background, both peaks and continuum, measured in the two MiDBD runs and was used to disentangle the origin of that measured with Cuoricino.

The major sources of the background observed in the  $0\nu\beta\beta$  region of interest were identified with multi-Compton events from the 2615 keV  $\gamma$  rays of  $^{2018}\text{Tl}$  and with ‘degraded  $\alpha$ s’. The former type of events was identified to be coming from the  $^{232}\text{Th}$  contamination of the cryostat, while the latter was attributed to surface contaminations of the TeO<sub>2</sub> crystals and of the material facing the detector, such as copper and PTFE frames. In fact, despite the kinetic energy of  $\alpha$ s (from U and Th daughters) is always far above the ROI, these particles can contribute to the background in the ROI if they loose only a limited fraction of their energy inside a single bolometer (without the possibility of reconstructing the total energy via coincidence analysis). This can happen when the contamination is localized on the surface either of the crystal or of the inert material closest to the detector (Fig. 14).

Above 2615 keV, a flat background continued up to 3900 keV (see the spectra in Figs. 12, 16, 18, 19 and 23). The only exception was the peak at 3249 keV of  $^{190}\text{Pt}$ , most likely due to an internal contamination of the crystals, since these were grown in platinum crucibles. At higher energies, above 4 MeV, the contribution of the various  $\alpha$  lines from the U and Th decay chains was found as expected. In particular, the region between 5 and 5.5 MeV was dominated by the  $^{210}\text{Po}$  contamination.

It is worth to notice that the position and the shape of



FIG. 15. Background study experimental setups. (Left) The RAD 1 (top) and RAD 3 (bottom) detectors. (Center) The CAW 1 (top) and CAW 3 (bottom) detectors. The composite bolometers for the rejection of surface radioactive background are visible at the bottom floors. (Right) The TTT detector top, middle and bottom towers. Adapted from Refs. [51, 86–88].

the  $\alpha$  peaks in the spectrum can provide a strong indication on the location of the contamination. In the case of Gaussian peaks, if the position corresponds to the transition energy of the decay ( $\alpha$  + nuclear recoil), this indicates that the contamination is internal to the crystal (bulk contamination). If the peak position corresponds to the  $\alpha$  energy, instead, this indicates that the contamination is within a thin layer on the surface of the crystal or of the inert material directly facing it (surface contamination). Long-tailed asymmetric peaks (on the low energy side) are due to thick contamination in the crystal surfaces, whereas a flat continuum (without peaks) is expected by either a bulk or a deep surface contamination of an inert material facing the detector.

In order to investigate the possible contributions to the background, especially the rather flat continuum between 3 and 4 MeV, and in view of the forthcoming CUORE, an intense R&D activity both in the material selection and in the surface cleaning procedure optimization was carried out. Therefore, in parallel with the Cuoricino running, many tests were performed in the Hall C facility.

#### 1. RAD detectors

A measurement campaign was performed with a dedicated setup, the Radioactivity Array Detector [87, 89] (RAD), with the aim of better understanding the con-

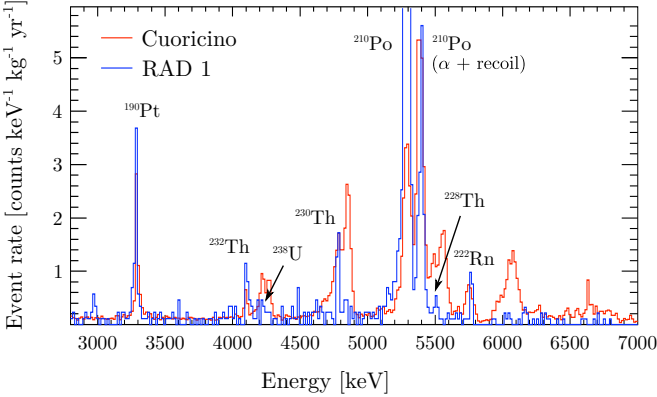


FIG. 16. Background comparison between Cuoricino (red) and RAD 1 (blue). The reduction of crystal surface contamination, still visible in the Cuoricino spectrum as large asymmetric peaks, is evident. Figure from Ref. [87].

tribution of the individual detector components. The RAD detector consisted of a 2 4-crystal floor array with a structure almost identical to that of Cuoricino (2 Cuoricino single modules, Fig. 15). The measurements, six in total, were carried out between summer 2004 and early 2007.

The purpose of the RAD 1 run was to define a new protocol for the surface cleaning. The crystals were etched and polished, while the copper structures etched and treated with electroerosion and only a few radioclean materials were allowed. The result was quite successful and saw the reduction of the  $^{238}\text{U}$  and  $^{232}\text{Th}$  peaks. In particular, the extremely low background allowed for the first time to disentangle the bulk from the surface contamination of the crystals, with the emerging of Gaussian peaks due to the internal contamination of  $\text{TeO}_2$  (Fig. 16). It was observed that the crystals were contaminated in Th isotopes, while no evidence of U contamination in secular equilibrium were obtained. The only other  $\alpha$  peaks were those of  $^{210}\text{Po}$  at 5.3 and 5.4 MeV, with intensities 3 times larger and comparable to Cuoricino, respectively. Finally, despite the strong reduction of the  $^{238}\text{U}$  and  $^{232}\text{Th}$  crystal contamination, no improvement was observed in the flat background over the (3 – 4) MeV region.

The RAD 2 run intended to test the background contribution coming from the “small parts” of the detector: the PTFE supports, the NTD, the heater and the gold bonding wires, glue and pins (used to attach the sensors to the crystal and to make the electrical connections). The top and bottom plates of the copper mounting structure were thus covered with samples of these part (a PTFE slab, a set of heaters and a set of gold wires). The results of this test were very clear. The (3 – 4) MeV rates measured proved that these materials together provided a maximum contribution to the Cuoricino (and RAD 1) background of  $\sim 20\%$ .

Remaining open the problem of the background reduction, the RAD 3 and 4 runs investigated the hypoth-

esis whether the source of the contaminations were actually degraded  $\alpha$ s. In order to do so, all the copper structure surfaces facing the crystals were covered with a radio-clean plastic layer. This would have stopped the  $\alpha$ s escaping from copper. Instead, nothing would have changed if the latter hypothesis was correct. At the same time, the contribution to the background from the thin foil could have been easily measured with a germanium detector since in this case bulk and surface contaminations were coinciding.

The obtained results showed that the crystal surface contaminations in  $^{238}\text{U}$  and  $^{232}\text{Th}$  were reduced by a factor  $\sim 4$  while the counting rate in the (3 – 4) MeV region of a factor  $\sim 2$ . Also, the 5.3 MeV  $^{210}\text{Po}$  peak, quite high in RAD 1, was ascribed to a contamination of the copper surface. In fact, this was efficiently reduced to a level compatible with Cuoricino thanks to the polyethylene film.

During RAD 4, a neutron shield was added to the cryostat external shielding. This was composed of an external 7 cm made of polyethylene for the thermalization of the fast neutrons, plus an internal thin layer made of boron carbide for the capture of the thermal neutrons. Dedicated measurements with an Am-Be source in the two configurations with and without the new shield allowed to test the neutron absorption capability. The results of RAD 4 were found completely compatible with those of RAD 3, thus indicating that environmental neutrons were not influencing the background in an appreciable manner.

Finally, the RAD 5 and 6 explored the possibility of exotic (non particle physics) effects as source of the contaminations, focusing in particular on the PTFE holders, which were therefore replaced with phosphorus-bronze clamps. The hypothesis was that, due the fast cool down, the PTFE could undergo internal adjustment once the cryostat base temperature was reached and it could therefore continue to release heat into the crystal absorber even for a long time, originating pulses that would mimic signal events. Unfortunately, a too high contamination of the clamps (probably due to  $^{210}\text{Pb}$ ) prevented from deducing anything about the exotic sources hypothesis. However, from the technical point of view, these last runs proved that the clamps could work in the same way of the PTFE supports.

In conclusion, the RAD tests confirmed the Cuoricino background model and proved the relevant role of the copper surface contamination in the in (3 – 4) MeV background region.

## 2. CAW detectors

In 2005 and 2006 a new design for the detector structure was tested. The prototype detector, the CUORE Assembling Working group (CAW) detector, consisted of a 3 4-crystal floor array (Fig. 15). The CAW detector was the result of an intense program of optimization of

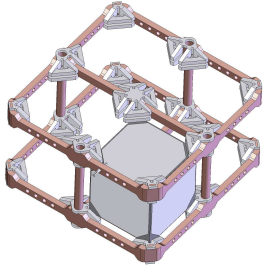


FIG. 17. Schematic of the CAW detector module. The same design for the copper frame and PTFE supports will be the base for the one used in CUORE (compare with Fig. 20). Figure from Ref. [86].

both the single module structure and its assembly procedure during the tower build up. The new structure reduced the amount of copper by a factor  $\sim 2$ . At the same time, the PTFE supports were moved on the vertices of the crystals. In the first attempt, used during the CAW 1 run, too much stress on the vertices actually caused cracks of the crystals. Therefore a further modification of the PTFE parts was implemented and used during the CAW 2 run (Fig. 17). The new structure relaxed the tension on the critical points, but introduced a larger amount of material. Considering that the hypothesis of thermal stress release from PTFE was still unsolved, in the end it was opted for smaller clamps, following the original idea, but adding small stress-relieving holes on the vertices to avoid the risk of cracks. This design became the official choice for CUORE and has always been ever since (see Fig. 20).

Concerning radioactivity, the CAW 1 test was a technical run, aimed at verifying the reproducibility and the effectiveness of the new setup. Therefore, no particular cleaning procedure for the setup was adopted, whereas this was done for the CAW 2 run. In this case, a RAD-like cleaning protocol (crystal surface and copper cleaned as for RAD 1 + copper covered with a polyethylene foil as for RAD 3) was adopted with the purpose of checking the background achievement obtained with the RAD runs in a different structure. With the CAW runs, the RAD results were confirmed, proving that the surface cleaning procedure of crystals and copper were reproducible (Fig. 18). The new measurements showed an easy, fast and standard assembling procedure. This improved the detector reproducibility and standardization.

As it can be seen from the pictures in Fig. 15 (central column), the bottom floors of the CAW detectors were covered with a slab of Ge and  $\text{TeO}_2$  during the CAW 1 and 2 runs, respectively. This was done in order to study the performance of prototype composite bolometers able to identify events originated at the detector surface, as R&D projects finalized at the background abatement (see Refs. [86, 90] for details).

During CAW 2, crystals coming from different producers were also checked. However, these were discarded since largely contaminated in  $^{232}\text{Th}$  and  $^{210}\text{Po}$ . SICCAS

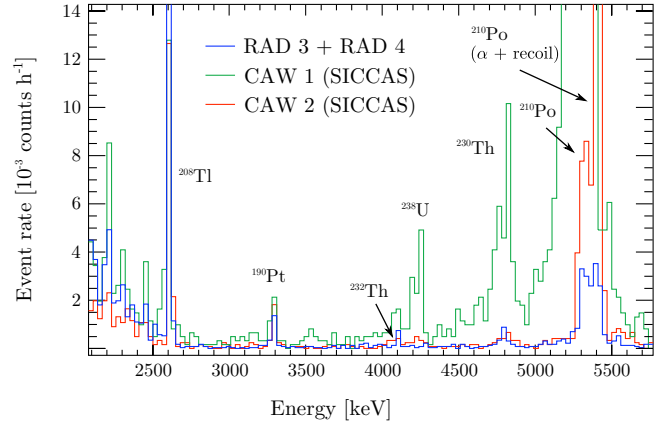


FIG. 18. Background comparison between RAD 3 + RAD 4 (blue), CAW 1 (green) and CAW 2 (red). In both the CAW cases, the spectra refer to the crystals produced by SICCAS. The comparable spectra of RADs and CAW 2 proves that the adopted surface treatment is reproducible. Figure from Ref. [87].

was thus confirmed as the producer for the CUORE crystals. The CAW detector was then used for the so-called Chinese Crystals Tests (CCTs) in order to validate a new production and treatment protocol for CUORE [47].

The CCT runs (two in total) aimed at verifying the crystal quality and the surface treatment on the way to CUORE. Up to Cuoricino, all the crystal surface cleaning procedure was performed in a clean room at LNGS. Moving to the direction of simplifying the cleaning operations, the CCTs intended to test the performance of the first crystals completely processed directly at SICCAS, where they had been grown. The surface treatment used in China (etching + lapping) was the same successfully optimized at the LNGS and verified with the RAD array.

In terms of bulk contamination, the CCTs showed limits that were comparable with those of Cuoricino, already sufficiently good for CUORE. Also, the repeated presence of a peak due to  $^{190}\text{Pt}$  consolidated the hypothesis of a possible inclusion of platinum fragments from the crucible used for the crystal growing (see the spectra in Figs. 16 and 18).

Regarding the surface contamination, instead, despite the measured levels for all the crystals were contained below the Cuoricino levels, the final sensitivity reached in the CCTs was not enough to establish whether the compliance with the requests for CUORE had been achieved.

### 3. TTT detector

In order to compare the results of different surface treatments of the copper frames, a higher statistics measurement than those of the RAD/CAW detectors was needed. Therefore, at the end of Cuoricino, the Hall A cryostat hosted the Three Tower Test (TTT) detector from September 2009 to January 2010 [51]. The

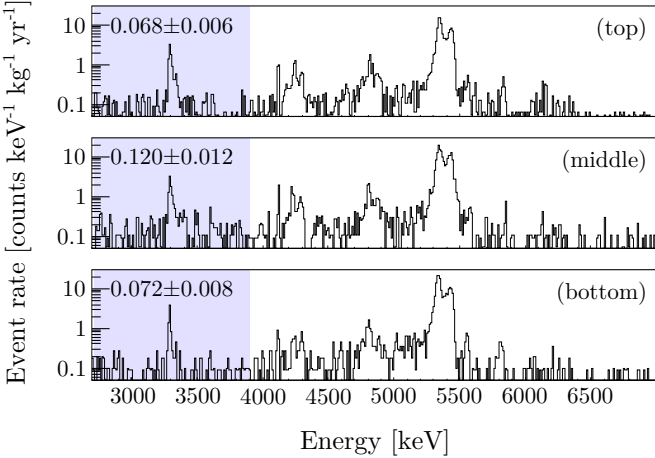


FIG. 19. Comparison of the TTT spectra in the  $\alpha$  region. The number of counts in the upper part of the plots refer to the  $(2700 - 3900)$  keV region (highlighted). The name in the brackets refer to the tower position in the detector. Figure from Ref. [51].

TTT detector consisted of 3 CAW-like arrays separated from each other by copper shields, for a total of 36 crystals, all coming from the Cuoricino production series (Fig. 15). To ensure similar contamination levels, history, and treatment, the crystal surfaces were all re-polished and the copper of the towers was taken from one single batch and machined following identical procedures.

The copper for the top tower was treated following the optimal protocol identified with the previous tests. This included a soap and chemical cleaning and the wrapping with multiple layers of polyethylene. The middle tower followed a new chemical process, starting from a simple soap cleaning and then adding electroerosion, chemical etching and passivation [91]. These two procedures were still done “manually” at LNGS. Instead, an “industrialized” cleaning procedure performed at the Laboratori Nazionali di Legnaro of I.N.F.N. (Legnaro (PD), Italy) was adopted for the bottom tower. In this case, the copper cleaning procedure consisted of tumbling, electro-polishing, chemical etching and magnetron plasma cleaning.

All these copper cleaning techniques led to significant reduction of the background in the flat background continuum compared to Cuoricino. The improvement was close to a factor  $\sim 2$  for the top and bottom towers, which got comparable results, while the rate of the central tower remained  $\sim 70\%$  higher (Fig. 19). Therefore, looking for the best compromise between cost, reproducibility and background control, the Legnaro protocol was validated for copper parts of the CUORE detector.<sup>10</sup>

#### 4. CCVRs

After the CCT runs and in parallel with the TTT measurement, the Hall C cryostat hosted the CUORE Crystal Validation Runs (CCVRs) [50]. The CCVRs, ten in total, were carried out between December 2008 and July 2013. These were cryogenic measurements designed to test the crystals produced by SICCAS upon their arrival at LNGS. Each time, four crystals randomly chosen from a batch were operated as bolometers in order to test the performance and the compliance to the strict radiopurity requests.

In general, all the measured values were compliant with the specification limits. The obtained results were satisfactory and a reduced background rate was observed with respect to Cuoricino over the whole energy range above 2700 keV. The upper limits for the bulk contamination of the crystals were set to  $5.3 \cdot 10^{-14}$  g/g for  $^{238}\text{U}$  and  $2.1 \cdot 10^{-13}$  g/g for  $^{232}\text{Th}$ . An upper value of few  $10^{-9}$  Bq cm $^{-2}$  could be instead set for the surface contamination of the same isotopes. Furthermore, an estimate of  $3.3 \cdot 10^{-6}$  Bq kg $^{-1}$  and  $1.0 \cdot 10^{-6}$  Bq cm $^{-2}$  on the activity of the bulk and surface contamination, respectively, of  $^{210}\text{Pb}$  (parent of  $^{210}\text{Po}$ ) could be set.

Starting from the obtained limits on the bulk and surface contamination, thanks to the CCVRs it was also possible to extrapolate (via Monte Carlo simulations) the contribution to the CUORE background arising from crystal impurities, studying its impact on the  $0\nu\beta\beta$  energy region (see Sec. V B 1).

#### D. Towards the tonne-scale

In Cuoricino, all the operations related to the detector assembly, e.g. the crystal surface treatments, the gluing and the bonding of sensors and heaters were still made handcraft. The same held for the tower wiring. This reflected in a quite broad range for the individual performance of the crystals. A standardization and automation of all the construction phases was needed for the handling of a detector almost 20 times bigger and much more complex as CUORE. At the same time, the high radiopurity levels of the components had to be conserved during (but also after) the various operations.

Therefore, completely new procedures were designed for the detector assembly and for the sensor gluing and bonding. The CUORE Tower Assembly Line (CTAL [92]) allowed to transform the over 10,000 ultra-clean pieces into 19 ultra-clean towers. To avoid re-contamination of all the parts due to direct contact with less radiopure materials and exposure to solid (any powder)

<sup>10</sup> Initially, it was decided to adopt a mixed approach for CUORE, with only the small copper parts to be subjected to the Legnaro protocol, while the large shields facing the external part

of the detector (MC shield and Tower Support Plate, refer to Fig. 25) had to be covered with polyethylene [51]. The final option consisted in substituting the polyethylene with copper tiles also cleaned according to the Legnaro protocol.

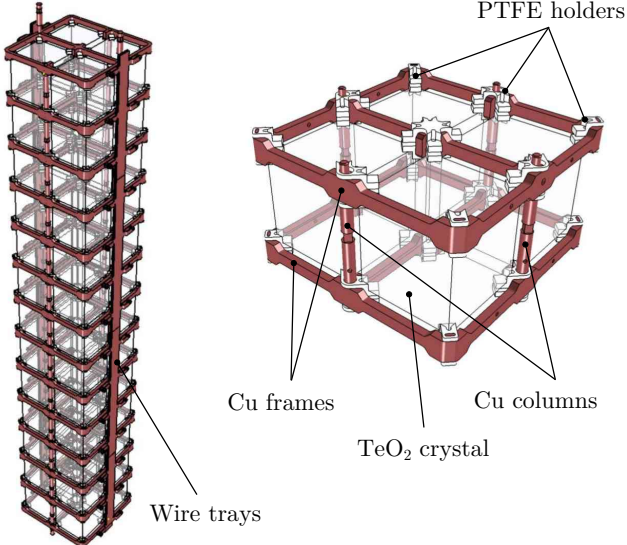


FIG. 20. Schematic of the CUORE-0 tower with a detail of a single floor, based on the CAW detector module ( $4.5 \times 5 \times 5 \text{ cm}^3$  crystals). Figure from Ref. [78].

or gaseous (Rn [93]) contaminants in the atmosphere, the whole CTAL process was confined into hermetic volumes constantly flushed with N<sub>2</sub>, accessible only through isolated glove ports. During all the handlings, the crystals were always vacuum sealed into plastic bags, in turn contained in vacuum sealed boxes. The sensor gluing was performed by means of a robotic arm for the crystal moving, a programmable xyz table and a glue dispenser, all inside an airtight N<sub>2</sub> flushed glove box [88]. Thermistors and heaters were thus pre-glued on the crystals. These then underwent the various operations: the mechanical assembly of the tower, the cabling, the bonding, the covering of the wire trays and the storage. In particular, the bonding (2 wires per pad for redundancy) could be now performed on the sensor and on the corresponding pad at the extremity of the wire tray at one time, thus avoiding any soldering material or mechanical contact. Regarding the detector wiring, the twisted-pair wires that were used up to Cuoricino (see Fig. 13) were substituted with Cu-PEN based flat flexible tapes [94, 95]. Thanks to the new procedures, the CUORE crystals were never exposed to air from the moment of the polishing to the installation of the detector.

To validate the ultraclean assembly techniques and to test the radiopurity of the materials for the upcoming CUORE, it was decided to run in the Hall A DR the first tower produced with the new protocol. This detector was thus called CUORE-0.

### 1. CUORE-0

CUORE-0 [78] was a tower made of 52  $50 \times 50 \times 50 \text{ mm}^3$  cubic crystal bolometers of  $\sim 750 \text{ g}$ , each disposed on

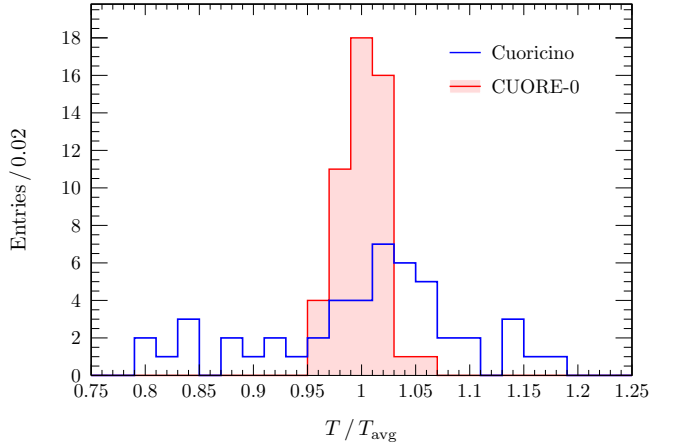


FIG. 21. Base temperatures of the individual bolometers normalized to their average temperature for Cuoricino and CUORE-0. The RMS of the distribution decreases from 9% to 2% passing from Cuoricino to CUORE-0. Figure from Ref. [78]

13 4-crystal floors, for a total mass of 39 kg of TeO<sub>2</sub> (Figs. 13 and 20).<sup>11</sup> It collected data from March 2013 until March 2015, with an interruption of about two months in September 2013 due to maintenance operations on the cryogenic system. The total duty cycle of the detector was close to 80%, of which about two thirds of physics data used for the  $0\nu\beta\beta$  analysis, with a <sup>130</sup>Te final exposure of 9.8 kg yr.

The CUORE-0 data allowed to directly verify the improvements achieved with the new CTAL, gluing and bonding procedures. With the new reproducible uniform assembly, the distribution of the single bolometer base temperature, which depends on the coupling between the thermistor, the absorber and the heat sink, narrowed the  $\Delta T$  RMS from the 9% of Cuoricino to 2% (Fig. 21). In terms of bolometric performance, CUORE-0 showed an improvement of the energy resolution with respect to its predecessor. The harmonic mean FWHM at  $Q_{\beta\beta}$  was  $(4.9 \pm 2.9)$  keV (Fig. 22). The CUORE goal, that was set to 5 keV FWHM in the ROI [96], had been reached.

Of course, the largest expectations concerned the background. CUORE-0 represented in fact the ultimate test on the effectiveness of the long background suppression program. A comparison of the CUORE-0 and Cuoricino spectra is shown in Fig. 23. The improvement spans over the whole energy range. In CUORE-0, a rate of  $(0.016 \pm 0.001)$  counts  $\text{keV}^{-1} \text{kg}^{-1} \text{yr}^{-1}$  was measured in the flat continuum of the  $\alpha$  region [97], a value about a factor 7 smaller than that obtained with Cuoricino,  $(0.110 \pm 0.001)$  counts  $\text{keV}^{-1} \text{kg}^{-1} \text{yr}^{-1}$  [85]. In particular, the  $\alpha$  continuum, that constituted the major contribution to the Cuoricino background in the

<sup>11</sup> Actually, the number of active bolometers was 51 since one NTD could not be bonded.

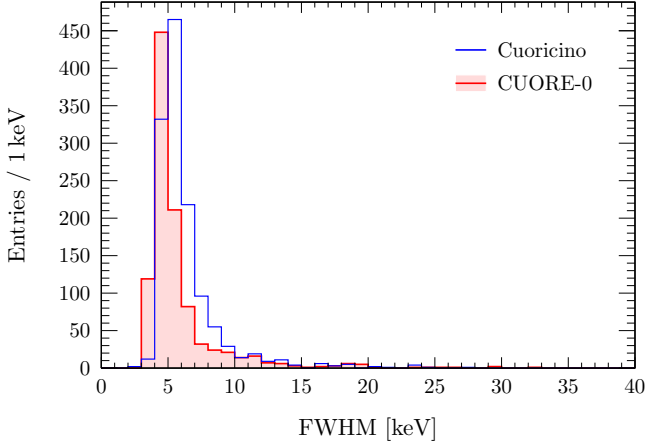


FIG. 22. Distribution of the FWHM energy resolution at the  $^{208}\text{Tl}$  line (2615 keV) for each Cuoricino and CUORE-0 dataset measured during the detector calibrations. The effective mean is 4.9 keV in CUORE-0, while it was 5.8 keV in Cuoricino. Figure from Ref. [78]

ROI, in CUORE-0 represented a minor component. The background rate in the  $Q_{\beta\beta}$  region was now  $(0.058 \pm 0.004 \text{ (stat.)} \pm 0.002 \text{ (syst.)}) \text{ counts keV}^{-1} \text{ kg}^{-1} \text{ yr}^{-1}$ , a factor almost 3 smaller than that obtained by the predecessor. As for CUORE, a major improvement in this region was still expected, thanks to the better material selection for its custom-made cryostat and to the scaling effects. By using the measured  $\alpha$  background index in CUORE-0 as an input to the Monte Carlo simulations of CUORE, it was possible to conclude that the background goal of 0.01 counts  $\text{keV}^{-1} \text{ kg}^{-1} \text{ yr}^{-1}$  was within reach [98].

## 2. CUORE

In the long way between the original proposal [80] and the actual detector construction, the design of CUORE has constantly evolved and improved thanks to the numerous studies and tests performed. In the final version [96], the array consists of 19 towers, for a total of 988  $\text{TeO}_2$  crystals and about 742 kg of weight, corresponding to  $\sim 206$  kg of  $^{130}\text{Te}$ . CUORE is by far the largest detector operated as a bolometer.

The full detector assembly took almost two years, going from September 2012 to July 2014. The successful completion of the task definitively proved the effectiveness of the CTAL, gluing and bonding protocols. Before being installed inside the CUORE cryostat, the towers had to wait the end of the commissioning of the cryogenic system [99]. Therefore, for other two years, these were stored inside the CUORE clean room into sealed containers constantly flushed with clean  $\text{N}_2$  gas to prevent any contamination from Rn. The tower installation took place during summer 2016. The extremely delicate operation was performed in a controlled clean room environment with Rn-free filtered air [100] by a specifically

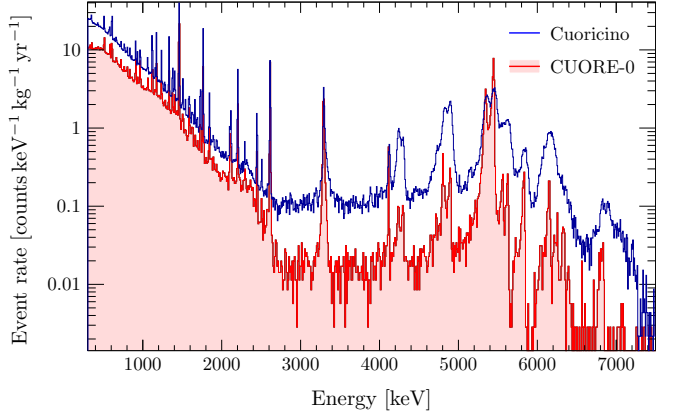


FIG. 23. Final spectra of Cuoricino and CUORE-0 in the (0 – 7.5) MeV region. The reduced background rate in CUORE-0 is clearly visible, especially in the  $\alpha$  region, where it is about a factor 7 smaller than in Cuoricino. Figure from Ref. [78]

trained team. A picture of the CUORE detector is shown in Fig. 24.

CUORE is expected to collect data for a total 5 yr of live-time. The design performance is 5 keV FWHM at  $Q_{\beta\beta}$ , while the target background level is 0.01 counts  $\text{keV}^{-1} \text{ kg}^{-1} \text{ yr}^{-1}$ , as a result of the extensive background reduction program and thanks to the new cryostat.

In fact, the CUORE detector could not be hosted in the Hall A DR or in any other standard one. A custom designed cryogenic system for CUORE had to be designed, realized and commissioned [99] in order to guarantee the optimal operation of the detector for a live-time of years, satisfying a set of very stringent experimental requirements in terms of high cooling power, low noise environment and low radioactivity content.

The adopted solution consisted in a large custom cryogen-free cryostat cooled by 5 (4 + 1 spare) Pulse Tube refrigerators (PTs [101]) and by a high-power  $^3\text{He}/^4\text{He}$  Dilution Unit [102, 103]. A schematic of the CUORE cryostat is shown in Fig. 25 (see also App. A). The CUORE cryostat comprises six nested vessels, the innermost of which encloses the experimental volume of about  $0.65 \text{ m}^3$ . To avoid radioactive background, only a few construction materials were acceptable and over 7 t of lead had to be cooled below 4 K. The lead shields include the Top Lead and the Internal Lateral and bottom Shield, the latter being made of ancient Roman lead. The Tower Support Plate holding the detector is attached to a dedicated suspension system in order to reduce the amount of vibrations and is placed right below the Top Lead. The whole cryostat is protected from the external radioactivity by the External Lateral and bottom Shield, a 18 cm polyethylene + 2 cm  $\text{H}_3\text{BO}_3$  + 25 cm lead shield on the side and 25 cm lead + 20 cm borated polyethylene shield on the bottom. In order to calibrate the detector while in operation, a dedicated system [104] had been integrated in the cryostat, allowing for the insertion and extraction



FIG. 24. The CUORE detector with the experiment logo [29].

of the sources without perturbing the cryogenic environment.

**CUORE first results** – After the cool down between December 2016 and January 2017 and the identification of suitable working conditions (operating temperature and bias voltages, see Sec. II D) the physics data-taking could finally begin in April 2017 [105]. The first results on the  $0\nu\beta\beta$  search, covering the interval between May and September 2017, for a total  $\text{TeO}_2$  exposure of 86.3 kg yr, have just been released [106]. These indicate that the target background has been reached, with the value of  $(0.014 \pm 0.002)$  counts  $\text{keV}^{-1} \text{kg}^{-1} \text{yr}^{-1}$  observed in the ROI. The average energy resolution of the detector at  $Q_{\beta\beta}$  is  $(7.7 \pm 0.5)$  keV improved during the data collection thanks to an optimization campaign performed on the detector. A further improvement down to  $\sim 5$  keV is foreseen by further optimizing the experimental operating conditions and through improvements of the analysis.

The successful commissioning and operation of CUORE mark a major step in the application of the bolometric technique and demonstrates the feasibility of future large-mass bolometer arrays for rare event searches.

#### IV. LIMITS ON THE $0\nu\beta\beta$ PROCESS

The observable that is probed by the experiments searching for the  $0\nu\beta\beta$  is the half-life of the decay  $t_{1/2}^{0\nu}$  of the isotope of interest.

In the fortunate event of a  $0\nu\beta\beta$  peak showing up in the energy spectrum, this parameter can be extracted

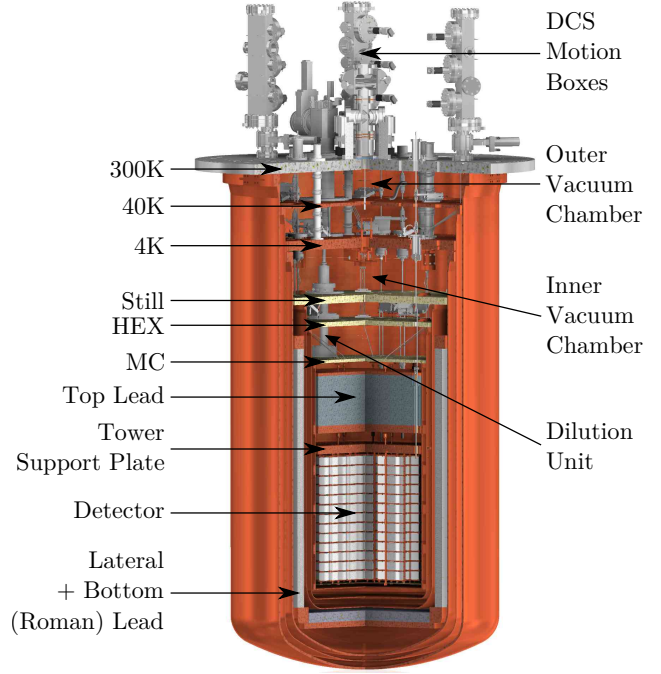


FIG. 25. Rendering of the CUORE cryostat. Figure from Ref. [104].

starting from the law of radioactive decay:

$$t_{1/2}^{0\nu} = \ln 2 / T \varepsilon \frac{N_{\beta\beta}}{N_{\text{peak}}} \quad (8)$$

where  $T$  is the measuring time,  $\varepsilon$  is the detection efficiency,  $N_{\beta\beta}$  is the number of  $\beta\beta$  decaying nuclei under observation, and  $N_{\text{peak}}$  is the number of observed decays in the peak.

If no peak is detected, the sensitivity of a given  $0\nu\beta\beta$  experiment,  $S_{1/2}^{0\nu}$ , is usually defined as the process half-life corresponding to the maximum signal that can be hidden by the background fluctuations  $n_B$  (at a given statistical C. L.). To obtain an estimate of this quantity as a function of the experiment parameters, we thus require that the  $0\nu\beta\beta$  signal exceeds the standard deviation of the total detected counts in the interesting energy window. At the confidence level  $n_\sigma$ , this means that we can write:

$$n_{\beta\beta} \geq n_\sigma \sqrt{n_{\beta\beta} + n_B} \quad (9)$$

where  $n_{\beta\beta}$  is the number of  $0\nu\beta\beta$  events and Poisson statistics for counts is assumed. If one now states that the background counts scale linearly with the mass of the detector,<sup>12</sup> from Eq. (8) it is easy to obtain the expres-

<sup>12</sup> This is true if impurities are uniform inside the detector. However, this might not be always the case. For example, if the main component of the background is superficial, it is the surface over volume ratio that matters.

sion:

$$S_{1/2}^{0\nu} = \ln 2 T \varepsilon \frac{n_{\beta\beta}}{n_\sigma \cdot n_B} = \ln 2 \varepsilon \frac{1}{n_\sigma} \frac{x \eta N_A}{\mathcal{M}_A} \sqrt{\frac{M T}{B \Delta}} \quad (10)$$

where  $B$  is the background level per unit mass, energy, and time,  $M$  is the detector mass,  $\Delta$  is the energy resolution,  $x$  is the stoichiometric multiplicity of the element containing the  $\beta\beta$  candidate,  $\eta$  is the  $\beta\beta$  candidate isotopic abundance,  $N_A$  is the Avogadro number and, finally,  $\mathcal{M}_A$  is the compound molecular mass. Despite its simplicity, Eq. (10) has the advantage of emphasizing the role of the essential experimental parameters.

When the background level  $B$  is so low that the expected number of background events in the ROI along the experiment life is close to zero, the expression of Eq. (10) is no more valid. It is the so called “zero background” experimental condition. The transition between the two regimes can be identified with the intermediate situation in which the expected number of counts is of the order of unity:

$$M T B \Delta = \mathcal{O}(1). \quad (11)$$

In this case,  $n_B$  is a constant (the maximum number of counts compatible with no observed counts, at a given C.L.) and the expression for the sensitivity becomes:

$$S_{1/2, 0\text{bkg}}^{0\nu} = \ln 2 T \varepsilon \frac{N_{\beta\beta}}{n_\sigma n_B} = \ln 2 \varepsilon \frac{x \eta N_A}{\mathcal{M}_A} \frac{M T}{N_s}. \quad (12)$$

The constant  $N_s$  is now the number of observed events in the ROI.

Reaching the zero background condition is a goal of the experimental searches since, in this case, the sensitivity grows much more rapidly (linearly with the exposure), as it can be seen by comparing Eqs. (10) and (12).

In Fig. 26, the zoom on the ROI region of the final MiDBD, Cuoricino and CUORE-0 spectra and of the first CUORE spectrum are shown. No evidence for the  $0\nu\beta\beta$  of  $^{130}\text{Te}$  has been found. However, these experiments allowed to set more and more stringent limits on the process (Fig. 27 and Table II). Starting from the early measurements almost thirty years ago, the evolution of the limit on the decay half-life of the  $0\nu\beta\beta$  of  $^{130}\text{Te}$  proceeded in parallel with that of the bolometric measurements. The first results presented to the scientific community were immediately competitive<sup>13</sup> and the subsequent improvements translated in an increase of sensitivity of several orders of magnitude.

<sup>13</sup> The most stringent limit on the inclusive double beta decay ( $0\nu\beta\beta + 2\nu\beta\beta$ ) of  $^{130}\text{Te}$  at the time of the 6 g crystal measurement (1991, see Sec. III A 1) was  $2.6 \cdot 10^{21}$  yr obtained with the

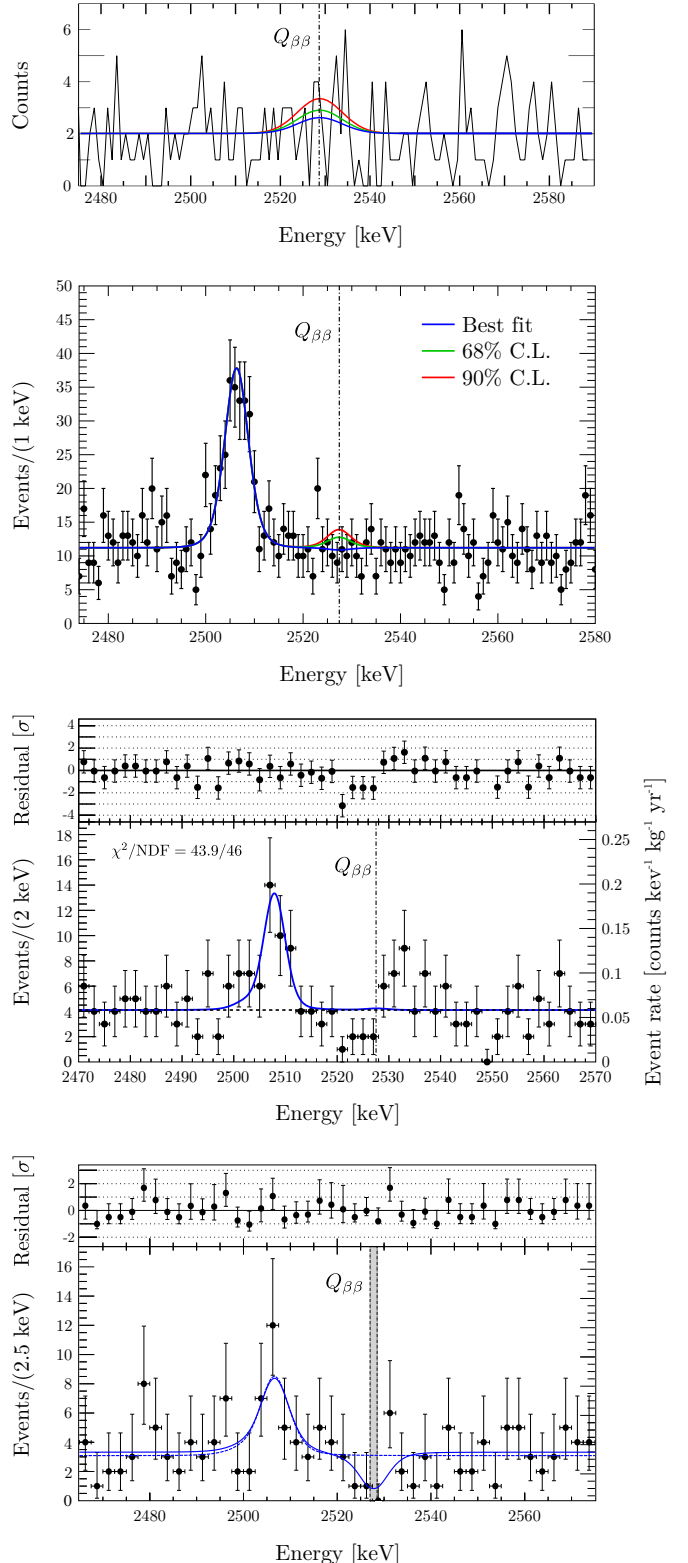


FIG. 26. (From Top to Bottom) MiDBD, Cuoricino, CUORE-0 and CUORE (first data release) best-fit model in the ROI overlaid on the data points. The peak at  $\sim 2507$  keV is attributed to  $^{60}\text{Co}$ . The vertical dot-dashed line indicates the position of the  $Q_{\beta\beta}$  of  $^{130}\text{Te}$ . Adapted from Refs. [71, 85, 106, 107] (see the references for details).

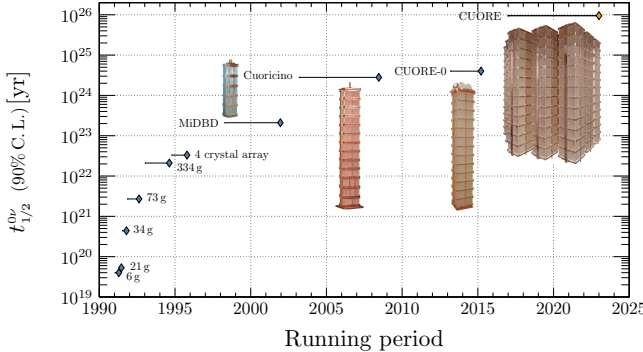


FIG. 27. Limits on the  $^{130}\text{Te}$   $0\nu\beta\beta$  half-life achieved by the described experiments. See Table II for the references.

Up to date, the limit on the  $^{130}\text{Te}$   $0\nu\beta\beta$  coming from CUORE (combined with CUORE-0 and Cuoricino) is  $1.5 \cdot 10^{25}$  yr [106]. It follows the limits on the analogous processes in  $^{136}\text{Xe}$  and  $^{76}\text{Ge}$ ,  $1.1 \cdot 10^{26}$  yr [110] and  $8.0 \cdot 10^{25}$  yr [111] at 90% C. L., respectively. CUORE is eventually expected to raise the half-life limit close to  $10^{26}$  yr [112], thus ensuring the central role of the search for  $0\nu\beta\beta$  of  $^{130}\text{Te}$  with thermal detectors also in the forthcoming future.

### A. Constraints on the neutrino masses

From the theoretical point of view, there can be different mechanisms originating the  $0\nu\beta\beta$  decay. Still, the general interest remains mostly focused on the *neutrino mass mechanism* [113]. Within this scenario, it is useful to define the so called Majorana effective mass:

$$m_{\beta\beta} \equiv \left| e^{i\alpha_1} |U_{e1}^2| m_1 + e^{i\alpha_2} |U_{e2}^2| m_2 + |U_{e3}^2| m_3 \right|. \quad (13)$$

The Majorana effective mass carries the information on the neutrino masses that can be extracted from the  $0\nu\beta\beta$  searches. In the definition of Eq. (13),  $m_i$  are the masses of the individual neutrinos  $\nu_i$ ,  $\alpha_{1,2}$  are the Majorana phases and  $U_{ei}$  are the elements of the mixing matrix that defines the composition of the electron neutrino:  $|\nu_e\rangle = \sum_{i=1}^3 U_{ei}^* |\nu_i\rangle$ . An experimental lower limit on  $t_{1/2}^{0\nu}$  can therefore be translated into a corresponding upper bound on  $m_{\beta\beta}$ .

In order to do so it is necessary to pass through quantities obtained by theoretical calculations of atomic and nuclear physics. Within the hypothesis of “ordinary”

---

geochemical method [108]. The tightest limit on  $0\nu\beta\beta$  from a direct measurement was instead  $2.8 \cdot 10^{18}$  yr from a measurement with a CdTe detector [7] (the result  $1.2 \cdot 10^{21}$  yr from Ref. [6] was overestimated since the energy resolution of the detector was not properly taken into account [7, 109]).

neutrinos as mediators of the  $0\nu\beta\beta$  transition, a convenient parametrization for  $t_{1/2}^{0\nu}$  can be:

$$\left[ t_{1/2}^{0\nu} \right]^{-1} = \frac{m_{\beta\beta}^2}{m_e^2} G_{0\nu} g_A^4 |\mathcal{M}_{0\nu}|^2 \quad (14)$$

where  $G_{0\nu}$  is the Phase Space Factor (PSF),  $\mathcal{M}_{0\nu}$  is the Nuclear Matrix Element (NME),  $g_A$  is the axial coupling constant and  $m_e$  is the electron mass, conventionally taken as a reference..

By inverting Eq. (14) and by choosing proper values for  $g_A$  and for the PSF [114] and NME [115] for  $^{130}\text{Te}$ , it is thus possible to obtain the new limits on  $m_{\beta\beta}$  starting from the experimental sensitivities reported in Table II (last column of the table).

To be fair, one should consider the uncertainties in the theoretical calculations while passing from  $t_{1/2}^{0\nu}$  to  $m_{\beta\beta}$ . The PSFs are known with accurate precision for the nuclei of interest. The present uncertainty is of about 7% [114]. For the NMEs, the situation is more complicated. A relatively small intrinsic error of  $\lesssim 20\%$  [115, 116] is presently assessed also for the NMEs by the most recent calculations. However, the disagreement between the results from different models is actually larger, up to a factor  $\sim 3$ , and when a process ‘similar’ to the  $0\nu\beta\beta$  is considered (single  $\beta$  decay, electron capture,  $2\nu\beta\beta$ ) and the calculations from the same models are compared to the measured rates, the actual differences are much larger than 20%. Finally, the value of  $g_A$  remains an open issue. The value measured in the weak interactions and decays of nucleons ( $g_{A,\text{nucl}} \simeq 1.27$ ) could indeed be “renormalized” in the nuclear medium toward the value appropriate for quarks ( $g_{A,\text{quark}} = 1$ ) or, even, the possibility of a further reduction (quenching) has been argued, based on the systematic over-prediction of the  $\beta$  and  $2\nu\beta\beta$  NMEs (worst scenario:  $g_{A,\text{phen}} \simeq g_{A,\text{nucl}} \cdot A^{-0.18}$ , where  $A$  is the mass number [117, 118]).<sup>14</sup>

In the idea of comparing the relative results, the value  $g_{A,\text{nucl}}$  and only one model for the NME are considered in Table II, nevertheless keeping in mind that these limits could vary and even worsen, especially in the case of quenching of  $g_A$ .

In Ref. [106] the official current CUORE limit of  $t_{1/2}^{0\nu} > 1.5 \cdot 10^{25}$  yr is converted into the limit  $m_{\beta\beta} < (140 - 400)$  meV at 90% C. L., depending on the nuclear matrix element employed (Fig. 31).

---

<sup>14</sup> If the latter was the case, the implications for the  $0\nu\beta\beta$  searches could be tremendous, given the strong dependence on  $g_A$  of the half-life [119, 120]. However, the answer depends on the source of the quenching, which is still unknown (see Ref. [121] for an extensive review on the topic). Also, some theoretical models find a dependence of  $t_{1/2}^{0\nu}$  on  $g_A$  milder than quartic, so that the effects of a suppression of this parameter are reduced [122, 123].

TABLE II. Limits on the  $0\nu\beta\beta$  half-life of  $^{130}\text{Te}$  and corresponding lower bounds for the Majorana effective mass. When comparable, the newer limits are combined with the old ones. In order to pass from  $t_{1/2}^{0\nu}$  to  $m_{\beta\beta}$ , the PSF from Ref. [114], the NME from Ref. [115] and  $g_{A,\text{nucl}}$  have been used.

Experiment	$t_{1/2}^{0\nu}$ (90% C. L.) [yr]	$m_{\beta\beta}$ [eV]
6 g crystal, [56]	$4.0 \cdot 10^{19}$	115
21 g crystal, [57]	$5.3 \cdot 10^{19}$	100
34 g crystal, [59]	$4.4 \cdot 10^{20}$	34
73 g crystal <sup>†</sup> , [63]	$2.7 \cdot 10^{21}$	14
334 g crystal, [65]	$2.1 \cdot 10^{22}$	5
4 crystal array, [66]	$3.3 \cdot 10^{22}$	4
MiDBD, [71]	$2.1 \cdot 10^{23}$	1.6
Cuoricino, [85]	$2.8 \cdot 10^{24}$	0.43
CUORE-0, [107]	$4.0 \cdot 10^{24}$	0.36
CUORE (first data), [106]	$1.5 \cdot 10^{25}$	0.19
CUORE (expected), [112]	$9.0 \cdot 10^{25}$	0.076

<sup>†</sup>only data from Run II were used for the  $0\nu\beta\beta$  analysis.

## V. CHALLENGES FOR A NEXT BOLOMETRIC DETECTOR

The future of the  $0\nu\beta\beta$  search with thermal detectors will not be concluded with CUORE. On the contrary, CUORE itself represents a fundamental step towards the next generation of detectors. The knowledge acquired by running the first tonne-scale bolometric array is of crucial importance to the understanding of how to further increase the sensitivity. It is thus possible to imagine a future  $0\nu\beta\beta$  experiment with improved performance to be placed inside the CUORE cryogenic infrastructure.

Bolometers offer a wide choice of possible absorber materials and thus isotopes different than  $^{130}\text{Te}$  can be in principle selected, thanks to their ‘intrinsic’ properties and/or to the more favorable characteristics of the resulting detector. This indeed represents a concrete possibility on the path towards a post-CUORE experiment (see Sec. V B 3 and Ref. [124]). Anyway, the following discussion will focus on  $\text{TeO}_2$ , since this remains a valid choice, with still much room for improvement towards a more powerful search for  $0\nu\beta\beta$ .

### A. Improving the sensitivity

As shown in Sec. IV, the probing power of the search for  $0\nu\beta\beta$  is determined by the experiment live-time, by the isotope mass, by the energy resolution and by the background level. These are thus the quantities that need to be addressed in order to try to improve the sensitivity. In particular, in the case of a next generation experiment, like the one we are considering, the aim is to reach the zero background condition, i. e. the relation expressed in

Eq. (11) must hold. This sets very stringent requirements on the detector features and performance.

In order to increase the mass of the isotope under study, it is necessary either to increase the whole detector mass or to enrich the detector material in that isotope (or both). In case of a future experiment inside the CUORE cryostat, it can be imagined that an optimization of the detector design will allow to allocate more material than in CUORE. However, this option is ultimately constrained by the experimental volume inside the cryostat. On the other side, the use of  $\text{TeO}_2$  crystals enriched in  $^{130}\text{Te}$  seems a viable path to be followed and the first results in this direction are promising. The recent run of two  $\text{TeO}_2$  enriched crystal ( $\sim 92\%$  of  $^{130}\text{Te}$ ) in the Hall C DR [125] proved that performance comparable to those of CUORE-0 are achievable. The crystals (of mass of  $\sim 435$  g each) showed a FWHM energy resolution at the  $^{208}\text{Tl}$  line of 6.5 and 4.3 keV, respectively. At the same time, the assessment of the crystal internal contamination indicated a relatively small presence of  $^{238}\text{U}$ , although (10 – 20) times larger than that of the CUORE crystals (see Sec. III C 4), while only an upper limit were obtained for  $^{232}\text{Th}$  (within a factor 2 with respect to the CUORE crystals). Therefore, it is possible to foresee a potential increase in the isotope mass up to a factor  $\sim 3$ .

Since it is unlikely that a  $0\nu\beta\beta$  experiment life will be longer than a few years, the optimization of the experiment duty cycle is another important factor in order to maximize the exposure. CUORE-0 already showed that values higher than 80% are achievable.<sup>15</sup> In addition, the use of PTs in the CUORE cryostat (see Sec. III D 2) further increases the total duty cycle with respect to a LHe bath cryostat (like the Hall A DR), due to the absence of cryogens to refill. It is thus reasonable to expect a duty cycle of  $\sim 80\%$  for a future experiment.

Regarding the resolution, bolometers fully exploit the potentiality of solid state detectors, showing values of the order of the per mille at the  $Q_{\beta\beta}$ , close to those of HPGe detectors. As discussed in Sec. II C, the effective resolution is due to various noise sources. In principle the intrinsic value for CUORE-like bolometers is of the order of some tens of eV. However, in order to try to improve the single detector performance, a better understanding of the bolometer behavior is crucial. Several studies aiming at building a working thermal model for the CUORE bolometers have been carried out over the years [72, 126, 127] and soon a large amount of data will be available thanks to CUORE, which will provide useful information in this direction. Anyway, since at present we do not know the level of improvement we can expect or how much time will be needed in order to obtain practical effects for the experimental search, no further improvement on this parameter will be considered. The value of

---

<sup>15</sup> The duty cycle of CUORE-0 was actually 78.6% [78]. However, this value includes the downtime between the two data taking campaigns (see Sec. III D 1).

$\sim 5$  keV already achieved by CUORE-0 still represents an acceptable target for a forthcoming experiment.

The suppression of the background is the target of most of the studies and R&D projects aiming at identifying the best configuration and technology for a new generation bolometric detector. This in fact is the key to reach the zero background condition and will actually represent the largest challenge to deal with. The good news is that there is still room for a significant improvement with respect to the  $0.01 \text{ counts keV}^{-1} \text{ kg}^{-1} \text{ yr}^{-1}$  of CUORE, as it will be discussed in the next section.

## B. Background suppression

In order to identify the most effective ways to reduce the background in a future experiment it is necessary to understand which are the actual contributions to the counting rate observed in CUORE. The natural starting point when dealing with this issue is represented by the Monte Carlo simulation already developed since MiDBD and continuously improved thereafter. In fact, thanks to the experiences acquired in running the subsequent detectors, especially Cuoricino and CUORE-0, this work allowed to project a background model for CUORE [98].

### 1. Contributions to the CUORE background

As discussed in Sec. III C, three dominant sources were identified by MiDBD and Cuoricino as contributors to the Background Index (BI), the event rate in the ROI (100 keV-wide region around the  $Q_{\beta\beta}$ , namely  $(2470 - 250)$  keV):

- the multi-Compton events from the 2615 keV  $\gamma$ s of  $^{208}\text{Tl}$  originating from the  $^{232}\text{Th}$  contamination of the cryogenic system;
- the  $^{238}\text{U}$  and  $^{232}\text{Th}$  contaminations (with the related decay products) on the surface of the  $\text{TeO}_2$  crystals, including the  $^{210}\text{Pb}$  surface implantation from the environmental  $^{222}\text{Rn}$ ;
- the  $^{238}\text{U}$  and  $^{232}\text{Th}$  contaminations (with the related decay products) on the surfaces of the inert materials facing the crystals, most likely of the copper holders.

This analysis guided the following strategies in view of CUORE, in particular the minimization of the amount of material used in the detector support structure, the design of the shields and dedicated cleaning treatments for both crystals and copper. Their effectiveness was proved by CUORE-0, which observed a  $\sim 2.6$  times reduced background with respect to Cuoricino (see Sec. IIID 1). In particular, this was found to be mainly imputable to the cryostat shields ( $\sim 74.4\%$  [21]), still the old ones of the Hall A DR.

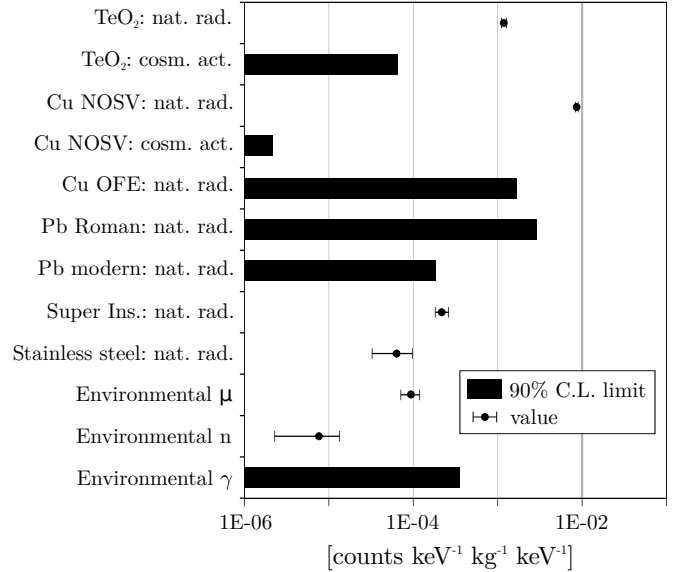


FIG. 28. Histogram representing the main BI expected for the various components of CUORE. The bars indicate 90% C.L. upper limits while the markers derived values (with the relative  $1\sigma$  uncertainty). The thicker line at  $0.01 \text{ counts } \text{keV}^{-1} \text{ kg}^{-1} \text{ yr}^{-1}$  indicate the goal for the CUORE background. Figure from Ref. [98] (see the reference for details).

In CUORE, an extensive screening campaign preceded the selection and procurement of the materials used in the construction not only of the detector, but also of the cryostat. Different material assay techniques allowed to deeply investigate the role of natural contaminants (especially  $^{238}\text{U}$  and  $^{232}\text{Th}$  with the respective progenies) and on cosmogenically activated contaminants ( $^{60}\text{Co}$ ,  $^{110}\text{Ag}$  and  $^{110m}\text{Ag}$  [128]) which are expected to yield a contributions in the ROI. The strict selection of the CUORE components took into account both bulk and surface contaminations, the latter possibly occurring during the part machining and cleaning, or during exposure to contaminated air.<sup>16</sup>

As a result of this work, the sources that give sizable contribution to the CUORE BI were identified with (Fig. 28):

- $^{238}\text{U}$  and  $^{232}\text{Th}$  and their progenies in crystals and holders;
- the cosmogenically activated isotopes in crystals and copper parts (both detector frames and Tower Support Plate + MC plate and vessel, see Fig. 25);
- $^{238}\text{U}$  and  $^{232}\text{Th}$  in the other vessels and in the lead shields.

<sup>16</sup> In addition, the break of the secular equilibrium of a radioactive chain could be relevant for surface contaminations as well, such as in the case of  $^{210}\text{Pb}$  from the  $^{238}\text{U}$  chain.

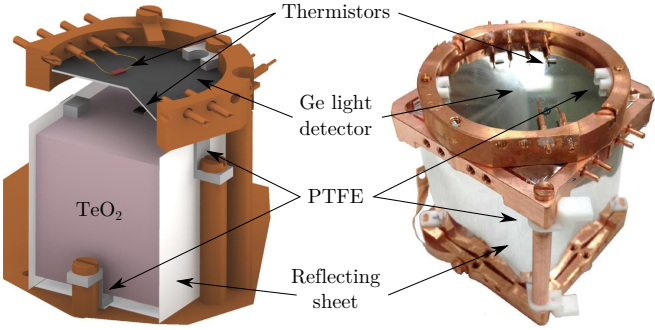


FIG. 29.  $\text{TeO}_2$  crystals coupled to a light detector for a simultaneous measurement of heat and light signals. The crystals are wrapped with a reflecting sheet in order to enhance the light collection. Adapted from Refs. [125, 129].

The total projected BI was found to be equal to  $(1.02 \pm 0.03 \text{ (stat)}^{+0.23}_{-0.10} \text{ (syst)}) \cdot 10^{-2} \text{ counts keV}^{-1} \text{ kg}^{-1} \text{ yr}^{-1}$  by far dominated by the degraded  $\alpha$  from surface contaminants of the detector frames. This value is perfectly compatible with the observed one of  $(0.014 \pm 0.002) \text{ counts keV}^{-1} \text{ kg}^{-1} \text{ yr}^{-1}$  [106].

As a remark, it is important to notice that the definitive validation or rejection of this projected background model for CUORE will come from the CUORE data themselves (with sufficiently high statistics). These will finally allow to disentangle the different contributions to the effective counting rate in the ROI.

## 2. Background active rejection

In CUORE,  $\alpha$  events and multi-Compton scatters of  $\gamma$ s are discarded mainly via anti-coincidence analysis, i. e. by rejecting simultaneous events (within 10 ms) generated in nearby crystals [106]. This method has a high efficiency, but it only allows to identify decays that deposit energy in multiple crystals.

Therefore, in view of a forthcoming detector, more sensitive approaches for active background reduction against  $\alpha$  events have been proposed. These foresee the use of a dual readout approach based on the simultaneous measurement of heat and light signals, the latter being collected by a thin Ge or Si slab coupled to the crystal and also employed as a bolometer (Fig. 29).

Scintillation light due to heavy particles is strongly quenched, thus the measurement of the ratio of the emitted light over the energy dissipated into heat allows to discriminate between  $\alpha$  and  $\beta/\gamma$  events with the same energy. Very good results in this direction have already been obtained (see e.g. Refs. [130–132]), however this approach is only limited to materials that exhibit scintillation properties. Therefore, the use of this techniques with  $\text{TeO}_2$  crystals is frustrated by the low luminescence

of paratellurite.<sup>17</sup>

Nonetheless, it was shown in Ref. [135] that  $\text{TeO}_2$  crystals have suitable optical properties to act as excellent Čerenkov radiators, with the threshold for Čerenkov emission of about 50 keV for electrons and of about 400 MeV for  $\alpha$  particles. Therefore, as in the case of scintillation, no light emission is expected from the  $\alpha$  background, allowing for a full background rejection, in principle even by detecting one single Čerenkov photon. A total of about 125 photons (in the range (350–600) nm) is expected for the two electrons emitted in the  $0\nu\beta\beta$  process and a light yield of about 52 Čerenkov photons per deposited MeV was actually measured in a CUORE-like crystal [136].

The Čerenkov emission from  $\text{TeO}_2$  was observed with dedicated measurements, first in a smaller [137, 138] and then in a full CUORE crystal [129]. The results showed that the discrimination of  $\alpha$  particles in CUORE is feasible. However, the collected light signal was too small. A higher sensitivity than that provided by standard bolometers is required in order to effectively apply an active discrimination in a future  $0\nu\beta\beta$  experiment, thus allowing for a drastic reduction of the background.

## 3. CUPID

Starting from the experience, the expertise, and the lessons learned in CUORE, the CUPID project (CUORE Upgrade with Particle IDentification [139]) aims at developing a future bolometric  $0\nu\beta\beta$  experiment with sensitivity on  $t_{1/2}^{0\nu}$  of the order of  $(10^{27} - 10^{28}) \text{ yr}$ .<sup>18</sup>

One of the main efforts of CUPID is devoted to the identification of effective strategies to reduce the background in the ROI, especially by developing high-resolution light detectors capable of clearly identifying Čerenkov emission. Several technologies are under investigation in this direction and many R&Ds programs are in different stages of evolution [140]. Among these, very promising solutions foresee the use of microwave kinetic inductance detectors [141, 142], transition edge sensors [143, 144] or Neganov-Luke amplified light detectors [125, 144–148]. In particular, the very recent results in Ref. [148] demonstrated a complete event-by-event  $\alpha$  vs.  $\beta/\gamma$  separation in a full  $\text{TeO}_2$  CUORE bolometer thanks to a Neganov-Luke-assisted Ge bolometer for the light detection (Fig. 30).

Complementary studies within CUPID focus on the tagging of surface events. In fact, due to the intrinsic

<sup>17</sup> Although in the end standard  $\text{TeO}_2$  was used, dedicated R&Ds studies, aiming at increasing the light emission in the crystals by mean of suitable dopants, had been performed for CUORE [133, 134].

<sup>18</sup> As introduced at the beginning of this section, the choice of an isotope different than  $^{130}\text{Te}$  is a possibility, but we will only consider the  $\text{TeO}_2$  case.

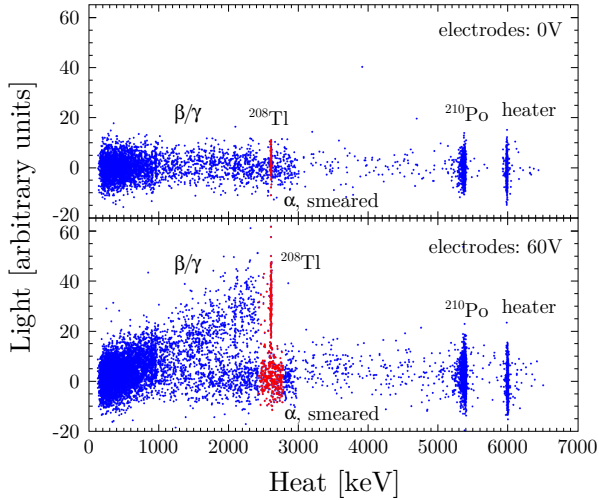


FIG. 30. Scatter plots of the heat *vs.* light signals in the measurements with a CUORE bolometer in coincidence with a Neganov-Luke Ge light detector operated respectively as a standard light detector (0 V electrode bias, Top) and in a signal amplification regime (60 V electrode bias, Bottom). Figure from Ref. [148] (see the reference for details).

working principle, bolometers do not have a dead layer and are fully sensitive up to the surface. While this property is responsible for the excellent energy resolution and high detection efficiency, it represents a problem when surface events represent a dominant component of the background, since the crystal surface is as sensitive as the bulk. In order to address this issue, the addition of passive elements on the bolometer surface has been proposed. The deposition of superconducting Al films should affect the shape of the events originating a few mm from the surface, thus one expects different signal shapes for surface and bulk events [149]. Alternatively, surface energy events could be identified thanks to an external plastic scintillator, by encapsulating the crystal with a scintillating foil and by adding a light detector to measure (in addition to the Čerenkov light) the light emitted in the interaction of surface events with the foil itself [150].

The proposed solutions, together with dedicated strategies for the reduction of the environmental radioactivity (see Ref. [140]), should translate into a reduction of the BI of 2 orders of magnitude with respect to CUORE, bringing it to the level of  $0.1 \text{ counts keV}^{-1} \text{ t}^{-1} \text{ yr}^{-1}$  and thus allowing the construction of a zero background (see Sec. IV) tonne-size bolometric experiment.

## VI. Te IN THE FUTURE OF THE $0\nu\beta\beta$ SEARCH

In the future of the  $0\nu\beta\beta$  search, the cost of the experiments will become a critical aspect to be taken into account. Most likely, no more than two isotopes will be selected to further continue the challenge. Therefore, it

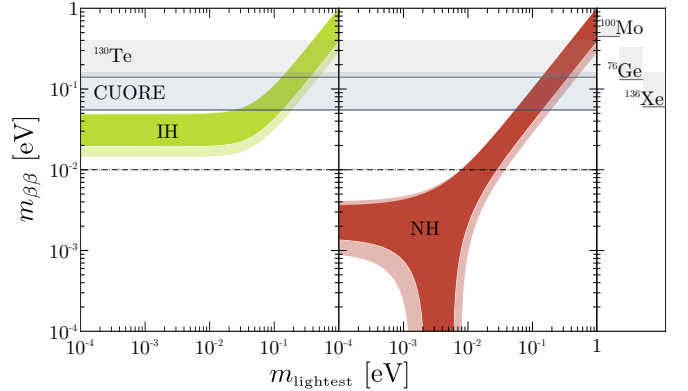


FIG. 31. Predictions on  $m_{\beta\beta}$  from oscillations with the related  $3\sigma$  regions [151] in the two cases of NH and IH. The horizontal bands show the current  $0\nu\beta\beta$  limit of  $^{130}\text{Te}$  [106] and the projected CUORE sensitivity [112]. The analogous limits on  $^{76}\text{Ge}$  [111],  $^{100}\text{Mo}$  [152] and  $^{136}\text{Xe}$  [110] are also reported. The line  $m_{\beta\beta} = 10 \text{ meV}$  indicates the target value for a future  $0\nu\beta\beta$  experiment capable of discriminating between NH and IH, as discussed in the text.

is important to understand the chances of  $^{130}\text{Te}$  to be selected as a suitable candidate.

Let us then try to infer some modest but fair considerations by comparing the case of  $^{130}\text{Te}$  with those of  $^{76}\text{Ge}$ ,  $^{100}\text{Mo}$  and  $^{136}\text{Xe}$ , that are at present setting the most stringent limits on  $0\nu\beta\beta$ . Following a similar argument to that presented in Ref. [120], let us imagine a (not too close) future experiment with enhanced sensitivity able to discriminate between the two scenarios of Normal and Inverted neutrino mass Hierarchies (NH and IH).

As discussed in Sec. IV A, in converting the experimental limit on the decay half-life time into the bound on the Majorana effective mass, it is necessary to pass through the theoretical calculations of nuclear physics which up to date present quite large uncertainties. Therefore, in order to consider different potential situations, we will assume small intrinsic uncertainties on the NMEs<sup>19</sup>, but different possibilities for the value of axial coupling constant. Namely we will use  $g_A$  equal to  $g_{A,\text{nucl}}$ ,  $g_{A,\text{quark}}$  and  $g_{A,\text{phen}}$ , hoping that at some point the issue of the quenching will be sorted out.

We will thus require the sensitivity to be equivalent to  $m_{\beta\beta} = 10 \text{ meV}$ . The corresponding limit on  $t_{1/2}^{0\nu}$  can be obtained by inverting Eq. (14). This situation is illustrated in Fig. 31, where  $m_{\beta\beta}$  is plotted against the mass of the lightest neutrino [154] (the current experimental

<sup>19</sup> In the following discussion, the value of  $\mathcal{M}_{0\nu}$  for each isotope (refer to Eq. (14)) has been obtained by averaging the individual ones from Refs. [115, 116, 153], while we will use the values from Ref. [114] for the PSFs.

TABLE III. Sensitivity and mass/cost of the isotope of a future experiment able to discriminate between NH and IH. The target is to probe  $m_{\beta\beta} = 10 \text{ meV}$ , assuming small uncertainties on the NMEs, and three possible values for  $g_A$  (see the text for details). The calculations are performed assuming zero background experiments (the required  $(B \cdot \Delta)$  product to fulfill this condition is reported) with 100% detection efficiency and no fiducial volume cuts.

Isotope	$G_{0\nu}$ [fyr $^{-1}$ ]	$\mathcal{M}_{0\nu}$	Price [\$/g]	$S_{1/2,0\text{bkg}}^{0\nu} [10^{28} \text{ yr}]$			M [t]			$(B \cdot \Delta)_{0\text{bkg}} [\text{t}^{-1} \text{ yr}^{-1}]$			Cost [M\$]		
				$g_{A,\text{nucl}}$	$g_{A,\text{quark}}$	$g_{A,\text{phen}}$	$g_{A,\text{nucl}}$	$g_{A,\text{quark}}$	$g_{A,\text{phen}}$	$g_{A,\text{nucl}}$	$g_{A,\text{quark}}$	$g_{A,\text{phen}}$	$g_{A,\text{nucl}}$	$g_{A,\text{quark}}$	$g_{A,\text{phen}}$
$^{76}\text{Ge}$	2.36	4.48	70	2.1	5.5	48	0.8	2.0	17.5	0.3	0.1	0.01	54	141	1230
$^{100}\text{Mo}$	15.9	4.51	100	0.3	0.8	8.6	0.1	0.4	4.1	1.3	0.5	0.05	15	39	410
$^{130}\text{Te}$	14.2	3.56	20	0.6	1.5	18	0.3	0.9	11.6	0.6	0.2	0.02	7	18	230
$^{136}\text{Xe}$	14.6	2.58	20	1.0	2.7	36	0.7	1.8	23.2	0.3	0.1	0.009	14	35	460

limits on the considered isotopes are reported as a comparison). It is worth to notice that assuming less favorable values for  $g_A$  is equivalent to require a higher sensitivities on  $m_{\beta\beta}$  with  $g_A = g_{A,\text{nucl}}$ . In particular, the case  $g_A = g_{A,\text{quark}}$  would corresponds to a goal  $m_{\beta\beta} \simeq 6 \text{ meV}$ , while the case  $g_A = g_{A,\text{phen}}$  to  $m_{\beta\beta} \simeq 2 \text{ meV}$ , more or less at the center of the NH for the lightest neutrino mass approaching zero.

By assuming 100% detection efficiency and no fiducial volume cuts and by fixing the live-time of the experiment (let's say to 5 yr), the required isotope mass to reach the target sensitivity can be extracted by inverting Eq. (12). Since this requires the zero background condition to be satisfied, the constraint expressed in Eq. (11) must hold.

The detector material is taken to be entirely made of the isotope of interest. Regarding the cost of the enrichment, there is large room for speculation and it is possible that the situation will significantly change in the future. However, it is realistic to assume that the minimum cost will be represented by that for the extraction of  $^{136}\text{Xe}$ , the easiest and least expensive isotope to separate since, being it in the gas form, it can directly undergo centrifugation. The current value amounts to 20\$ per gram of isotope [9].<sup>20</sup> A similar cost can be assumed for  $^{130}\text{Te}$  [24], while larger ones have to be considered for  $^{76}\text{Ge}$  and  $^{100}\text{Mo}$  [155].

The result is shown in Table III. It can be seen that in terms of affordability,  $^{130}\text{Te}$  is the most convenient isotope. The cost of its procurement for an experiment would be half of that of  $^{100}\text{Mo}$  or  $^{136}\text{Xe}$  and about 1/8 of  $^{76}\text{Ge}$ . The isotope cost could become critical for  $^{76}\text{Ge}$  already in the most favorable  $g_A$  case and most likely overwhelming in the intermediate one, while still acceptable for the other candidates. In the worst scenario or, equivalently probing the NH in more favorable conditions,  $^{130}\text{Te}$

is the only isotope that still gets a chance, if any will exist. Anyway, it is fair to say that this generic indications do not take into account the cost of the whole experimental infrastructure and the feasibility of constructing and running such an experiment, especially in the zero background condition.<sup>21</sup>

Considering the specif case of bolometric  $\text{TeO}_2$  experiment, the amount of material and the background requirements in the first scenario will be likely fulfilled by CUORE (see Sec. V B 3), while in the case of  $g_A = g_{A,\text{quark}}$  a larger effort would be needed, but still it could be considered an open challenge.

## VII. SUMMARY

Neutrinoless double beta decay is a key tool to address some of the major outstanding issues in neutrino physics, such as the lepton number conservation and the Majorana nature of the neutrino. Thermal detectors based on  $\text{TeO}_2$  fulfill the requirements for a competitive experiment searching for this rare process. In their almost thirty years old history, these devices have achieved very important results, setting more and more stringent constraints on the decay half-life of the  $0\nu\beta\beta$  of  $^{130}\text{Te}$ . The present limit on this process obtained by CUORE,  $1.5 \cdot 10^{25} \text{ yr}$  at 90% C. L., is among the most competitive ones on the  $0\nu\beta\beta$ .

Table IV summarizes the main features of the chain of bolometric experiments presented in this work.<sup>22</sup> The series of significant improvements appears here evident. Passing from the 6 g crystal to CUORE, the detector mass has increased of more than a factor  $10^5$ . At the

<sup>20</sup> Actually, the cost of enrichment is proportional the ratio of the output and input isotopic abundances and the process almost never reaches 100% extraction. Anyway, for the sake of the present discussion, it is acceptable to approximate the enrichment to ‘complete’ process fully separating the isotope of interest.

<sup>21</sup> Up to date, only GERDA has achieved a low enough BI that would fulfill the requirement for a zero background equivalent experiment of about 1 t [156].

<sup>22</sup> To allow the direct comparison of the different parameters, some slight imprecision on the original values could have been introduced. This holds in particular for the older experiments.

TABLE IV. List of the  $\text{TeO}_2$  bolometric experiments searching for the  $0\nu\beta\beta$  of  $^{130}\text{Te}$  performed at LNGS. The main characteristics are reported.

Experiment	Running period	Crystals	Mass [kg]	Exposure <sup>†</sup> [kg yr]	BI in ROI [counts $\text{keV}^{-1} \text{kg}^{-1} \text{yr}^{-1}$ ]	FWHM @ $Q_{\beta\beta}$ [keV]
6 g crystal, [56]	Jan 1991 - Apr 1991	1	0.006	0.0002	123	50
21 g crystal, [57]	May 1991 - Jun 1991	1	0.021	0.0004	88	20
34 g crystal, [59]	Jul 1991 - Oct 1991	1	0.034	0.0041	79	40
73 g crystal, [63]	Nov 1991 - Aug 1992	1	0.073	0.0087	35 (Run I) / 17 (Run II)	7
334 g crystal, [64, 65]	Jan 1993 - Aug 1994	1	0.334	0.40	3.4	15
4 crystal array, [66]	Oct 1994 - Oct 1995	4	1.32	0.73*	4	$\lesssim 12$
MiDBD, [71]	Apr 1998 - Dec 2001	20	6.8	4.25	0.6 (Run I) / 0.3 (Run II)	5 - 15
Cuoricino, [85]	Mar 2003 - Jun 2008	62	40.7	71.4	0.20 (Run I) / 0.15 (Run II)	$5.8 \pm 2.1^{\ddagger}$
CUORE-0, [78, 107]	Mar 2013 - Mar 2015	52	39.0	35.2	$0.058 \pm 0.004$	$4.9 \pm 2.9$
CUORE (expected), [96]	Apr 2017 - 2023	988	742	3705	0.01	5

<sup>†</sup>Total exposure of  $\text{TeO}_2$ . To get the corresponding exposure of  $^{130}\text{Te}$ , it is sufficient to multiply the value per  $\simeq 0.278$ .

\* combined with 334 g crystal.

<sup>§</sup>[78].

same time the background rate has been constantly reduced and the resolution improved, reaching values comparable with those of the best performing detectors. CUORE is expected to fully exploit the potentiality of the calorimetric technique. The strict protocol designed for the detector construction is the results of an extensive and continuous R&D program, while the cryogenic system represents a milestone in the dilution refrigeration technology. The successful operation of CUORE has opened the way to one of the most sensitive searches for  $0\nu\beta\beta$  and to the possibility for tonne-scale bolometric experiments.

Looking towards a next generation bolometric experiment searching for  $0\nu\beta\beta$ , there is still room for a significant improvement in the detector sensitivity. The numerous R&D projects are showing promising results on the way of a complete particle identification, thus leading to a strong suppression of the background. The construction of a zero background experiment seems within the reach. It is fair to imagine that such a detector will reach sensitivities of the order of  $(10^{27} - 10^{28}) \text{ yr}$ .

Within the worldwide contest of the search for  $0\nu\beta\beta$ ,  $^{130}\text{Te}$  represents one of the most favorable candidates and it is likely that bolometric detectors will continue to play a crucial role in this challenge.

## ACKNOWLEDGMENTS

The present review is a re-elaboration of a thirty-year history of research activities. The reported scientific material comes from original works published initially by the group of Fiorini and Collaborators and later by the Cuoricino and CUORE Collaborations. The achieved results have been made possible by the dedication and efforts by these Physicists and of the Technical Staff of the

Laboratori Nazionali del Gran Sasso and other Institutions.

## APPENDIX A: Cryogenics apparatus

In order to operate a bolometric detector, a system able to reach and maintain a stable working temperature of  $\sim 10 \text{ mK}$  for long periods is needed. The (only possible) solution is found in the use of a Dilution Refrigerator (DR).

A DR is a cryogenic device whose working principle relies on the  $^3\text{He}/^4\text{He}$  mixture properties. The original idea was suggested by London in 1951 [157] and, about ten years later, the same London, Clarke and Mendoza published a proposal for realizing such a cooling system [158]. The first functioning DR was built in 1965 [159] and steady improvements followed since then, leading to the lowest (stable) temperatures of  $2 \text{ mK}$  in 1978 [160] and of  $1.75 \text{ mK}$  in 1998 [161].

Since the late 1960s, it has also become possible to buy commercial DRs. This is the case for the cooling units used for the measurements described in this work (see Sec. III A). Today, “plug and play” DRs are on the market, thus avoiding the need of a deep knowledge of cryogenics to use these very delicate devices.

### 1. DR working principle

Let us consider the properties of the  $^3\text{He}/^4\text{He}$  mixture. We refer to Fig. 32, in which the concentration *vs.* temperature diagram for the liquid  $^3\text{He}/^4\text{He}$  mixture at saturated vapor pressure is shown.

Liquid  $^4\text{He}$  becomes super-fluid at  $T = 2.177 \text{ K}$ , while  $^3\text{He}$  does not show any phase transition down to some

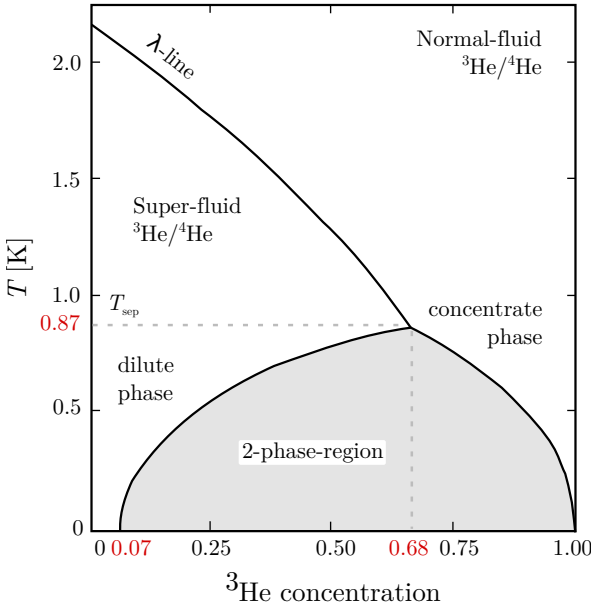


FIG. 32. Phase diagram of liquid  ${}^3\text{He}/{}^4\text{He}$  mixture at saturated vapor pressure. The  $\lambda$ -line for the super-fluid transition of  ${}^4\text{He}$  separates into two for  $T = T_{\text{sep}}$  and sufficiently high concentration of  ${}^3\text{He}$ . Below this temperature the two isotopes separate into a  ${}^4\text{He}$  and a  ${}^3\text{He}$  rich phase). Adapted from Ref. [162].

millikelvin. However, the temperature of the super-fluid phase transition of the (Bose) liquid  ${}^4\text{He}$  decreases if this is dilute into the (Fermi) liquid  ${}^3\text{He}$ . Eventually, the  ${}^4\text{He}$  super-fluidity ceases to exist for  ${}^3\text{He}$  concentrations greater than 67.5% [162]. At this concentration and at  $T = T_{\text{sep}} \equiv 0.867\text{ K}$  the  $\lambda$ -line, i.e. the transition line between the  ${}^4\text{He}$  normal-fluid and super-fluid phases, separates into two. Below this temperature, the two isotopes are only miscible for fixed concentrations depending on the temperature. This means that the shaded region in the figure is not physically accessible.

If we cool a  ${}^3\text{He}/{}^4\text{He}$  mixture to temperatures below  $T_{\text{sep}}$ , therefore, the liquid will separate into two phases, one rich in  ${}^3\text{He}$  and the other rich in  ${}^4\text{He}$  (dilute in  ${}^3\text{He}$ ). In particular, due to its lower density, the  ${}^3\text{He}$ -rich liquid will float over the  ${}^4\text{He}$ -rich liquid. Close to  $T = 0\text{ K}$ , the former is almost pure  ${}^3\text{He}$ . Instead, the  ${}^3\text{He}$  concentration in the latter never drops to zero, but it reaches a constant concentration of  $\sim 6.6\%$  and this finite solubility is at the base DR technology.

Since the  ${}^3\text{He}$  vapor pressure is much higher than the  ${}^4\text{He}$  one, by pumping on the  ${}^4\text{He}$ -rich phase it is possible to extract almost only  ${}^3\text{He}$ , thus destroying the equilibrium in the concentration ratio. To restore the equilibrium, the  ${}^3\text{He}$  from the concentrate phase has to cross the phase boundary to the dilute phase. However, since the enthalpy of  ${}^3\text{He}$  in the dilute phase ( $H_d$ ) is larger than the enthalpy of  ${}^3\text{He}$  in the concentrate one ( $H_c$ ), we have a cooling power occurring at the phase separation line when  $\dot{n}_3$  moles of  ${}^3\text{He}$  per unit time are transferred

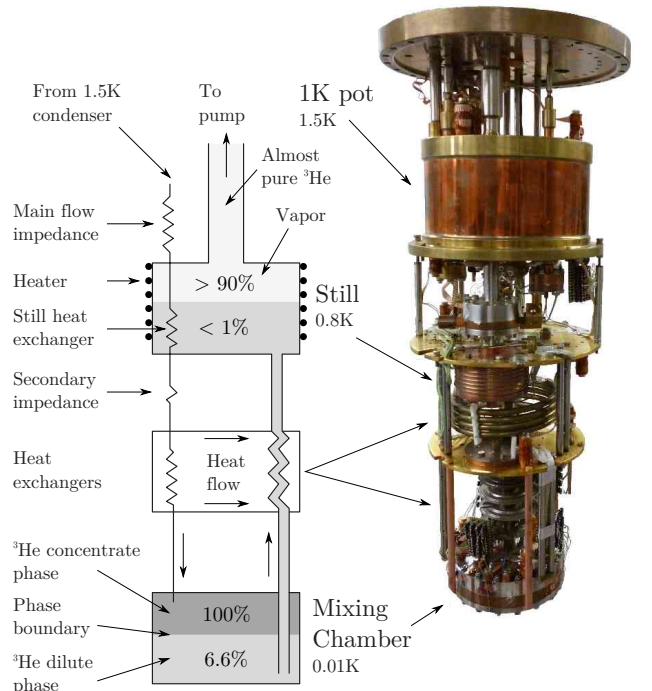


FIG. 33. (Left) Scheme of the inner circuit of a DR. Adapted from Ref. [30]. (Right) Picture of the DR presented in Ref. [53] (see Sec. III A).

from the concentrate to the dilute phase [162]:

$$\dot{Q} = \dot{n}_3 [H_d(T) - H_c(T)] \simeq 84 \dot{n}_3 T^2. \quad (\text{A1})$$

Typical values for  $\dot{Q}$  for DR working at  $\sim 10\text{ mK}$  are of the order of few  $\mu\text{W}$ .

A detailed (and quantitative) description of the operation of a DR can be found in Refs. [30, 162].

## 2. Schematic representation of a DR

To exploit the cooling properties of the  ${}^3\text{He}/{}^4\text{He}$  mixture, a preliminary cooling is needed in order to reach  $T = T_{\text{sep}}$ , where the phase separation takes place.

A first step consists in cooling down the DR to about 4 K. With the older devices, this is usually done by “dipping” the DR itself into a liquid  ${}^4\text{He}$ -bath ( $T = 4.22\text{ K}$ ). This is indeed the case for the ones used for the measurements described in this work. More recent DR use cryo-coolers and, in particular PTs, [163], to reach approximately the same temperature. PTs avoid the need of a  ${}^4\text{He}$ -bath cryostat with its infrastructure, guarantee a high reliability and, due to the absence of cryogens to refill, increase the total duty cycle of the experiment, thus allowing a longer live-time.

The cool down of the incoming mixture to approximately  $(1 - 1.5)\text{ K}$  in cryogen-based DR is realized by an evaporation refrigerator usually called 1K pot. This is

filled through a capillary by the same LHe from the  $^4\text{He}$ -bath. By pumping the vapor above the liquid inside the 1K pot, the temperature decreases. In cryogen-free DR, instead, the incoming mixture is cooled down to  $< 1\text{ K}$  thanks to the Joule-Thomson effect. In both cases, this cooling phase is fundamental to condense the mixture.

The core of a DR essentially consists of three elements: the Mixing Chamber (MC), the Still and the Heat EX-changers (HEXs). This part of the apparatus is located in an inner vacuum chamber (also containing the 1K pot or the Joule-Thomson impedance). A schematic representation and an example of real version are shown in Fig. 33. The relatively complex  $^3\text{He}/^4\text{He}$  circuit is necessary to guarantee a sufficiently high circulation of  $^3\text{He}$ , while maintaining a low heat load on the MC. The circulation of the mixture is driven by pumping the Still, which is heated to about  $0.7\text{ K}$  to increase the pumping efficiency. Due to the higher vapor pressure,  $^3\text{He}$

is predominantly evaporated from the liquid, although its concentration in the liquid in the Still is only  $\sim 1\%$ . Once it has been pumped, the  $^3\text{He}$  is returned to the cryostat (after being cleaned in a nitrogen trap). After the 1K pot (or the Joule-Thomson impedance), where a first condensing of the gas takes place thanks to a flow impedance, the  $^3\text{He}$  is led into a series of counterflow HEXs. After passing through the HEXs, it enters the MC. The return line to the Still starts in the MC below the phase boundary (in the  $^4\text{He}$ -rich phase). On the way back to the Still, the cold mixture again flows through the HEXs and in this way pre-cools the incoming  $^3\text{He}$ . By pumping the Still, a concentration gradient of  $^3\text{He}$  is created and this leads to an osmotic pressure that causes  $^3\text{He}$  to flow from the MC to the Still. The cross of the phase boundary by the  $^3\text{He}$  atoms in the MC cools down the system.

- 
- [1] W. H. Furry, *Phys. Rev.* **56**, 1184 (1939).
  - [2] E. Majorana, *Nuovo Cim.* **14**, 171 (1937).
  - [3] G. Racah, *Nuovo Cim.* **14**, 322 (1937).
  - [4] A. Giuliani and A. Poves, *Adv. High Energy Phys.* **2012**, 857016 (2012).
  - [5] S. Das, S. K. Ghorui, P. K. Raina, A. K. Singh, P. K. Rath, F. Cappella, R. Cerulli, M. Laubenstein, P. Belli and R. Bernabei, *Nucl. Instrum. Meth. A* **797**, 130 (2015).
  - [6] Y. G. Zdesenko, *JETP Lett.* **32**, 58 (1980).
  - [7] L. W. Mitchell and P. H. Fisher, *Phys. Rev. C* **38**, 895 (1988).
  - [8] R. Arnold *et al.* (NEMO-3 Collaboration), *Phys. Rev. Lett.* **107**, 062504 (2011).
  - [9] S. D. Biller, *Phys. Rev. D* **87**, 071301 (2013).
  - [10] S. P. Langley, *Proc. Am. Acad. Arts Sci.* XVI, 342 (1881).
  - [11] P. Curie and A. Laborde, *C. R. Acad. Sci.* **136**, 673 (1903).
  - [12] D. H. Andrews, R. D. Fowler and M. C. Williams, *Phys. Rev.* **76**, 154 (1949).
  - [13] F. Simon, *Nature* **135**, 763 (1935).
  - [14] G. V. Mitsel'makher, B. S. Neganov and V. N. Trofimov, (1982), [Communication to the Joint Institute for Nuclear Research, Dubna, Russia, P8-32-549].
  - [15] E. Fiorini and T. O. Niinikoski, *Nucl. Instrum. Meth. A* **224**, 83 (1984).
  - [16] A. Drukier and L. Stodolsky, *Phys. Rev. D* **30**, 2295 (1984).
  - [17] S. H. Moseley, J. Mather and D. McCammon, *J. Appl. Phys.* **56**, 1257 (1984).
  - [18] S. Rahaman *et al.*, *Phys. Lett. B* **703**, 412 (2011).
  - [19] M. Redshaw, B. J. Mount, E. Myers and F. T. Avignone, *Phys. Rev. Lett.* **102**, 212502 (2009).
  - [20] N. D. Scielzo *et al.*, *Phys. Rev. C* **80**, 025501 (2009).
  - [21] C. Alduino *et al.* (CUORE Collaboration), *Eur. Phys. J. C* **77**, 13 (2017).
  - [22] M. A. Fehr, M. Rehkamper and A. N. Halliday, *Int. J. Mass Spectrometry* **232**, 83 (2004).
  - [23] <https://www.metalprices.com> (2016).
  - [24] Private communication with Prof. F. Avignone (2017).
  - [25] <https://www.lngs.infn.it/en>.
  - [26] P. G. Catalano, G. Cavinato, F. Salvini and M. Tozzi, *Mem. Soc. Geol. It.* **35**, 647 (1986).
  - [27] M. Ambrosio *et al.* (MACRO Collaboration), *Phys. Rev. D* **52**, 3793 (1995).
  - [28] A. Best, J. Görres, M. Junker, K. L. Kratz, M. Laubenstein, A. Long, S. Nisi, K. Smith and M. Wiescher, *Nucl. Instrum. Meth. A* **812**, 1 (2016).
  - [29] <https://cuore.lngs.infn.it/en>.
  - [30] C. Enss and H. Siegfried, *Low-Temperature Physics* (Springer, 2005).
  - [31] H. C. Stahl, *Cryogenic Particle Detection* (Springer, 2005).
  - [32] E. E. Haller, N. P. Palaio, M. Rodder, W. L. Hansen and E. Kreysa, in *Neutron Transmutation Doping of Semiconductor Materials*, edited by R. D. Larabee (Springer US, 1984) pp. 21–36.
  - [33] C. Erginsoy, *Phys. Rev.* **80**, 1104 (1950).
  - [34] N. F. Mott, *Philos. Mag.* **19**, 835 (1969).
  - [35] B. I. Shklovskii and A. L. Efros, *Electronic Properties of Doped Semiconductors* (Springer, 1984).
  - [36] M. Barucci, C. Brofferio, A. Giuliani, E. Gottardi, I. Peroni and G. Ventura, *J. Low Temp. Phys.* **123**, 303 (2001).
  - [37] J. Mather, *J. Appl. Optics* **21**, 1125 (1982).
  - [38] J. Mather, *J. Appl. Optics* **23**, 584 (1984).
  - [39] A. Alessandrello *et al.*, *Nucl. Instrum. Meth. A* **412**, 454 (1998).
  - [40] C. Arnaboldi, A. Giachero, C. Gotti and G. Pessina, *Nucl. Instrum. Meth. A* **652**, 306 (2011).
  - [41] E. Andreotti, C. Brofferio, L. Foggetta, A. Giuliani, B. Margesin, C. Nones, M. Pedretti, C. Rusconi, C. Salvioni and M. Tenconi, *Nucl. Instrum. Meth. A* **664**, 161 (2012).
  - [42] W. Dutton, W. A. Charles Cooper, *Chem. Rev.* **66**, 657 (1966).
  - [43] G. K. White, S. Collocott and J. G. Collins, *J. Phys. Condensed Matter* **2**, 7715 (1990).
  - [44] F. R. Kroeger and C. A. Swenson, *J. Appl. Phys.* **48**,

- 853 (1977).
- [45] R. A. H. El-Mallawany, *Tellurite Glasses Handbook: Physical Properties and Data* (CRC Press, 2002).
- [46] Y. Chu, Y. Li, Z. Ge, G. Wu and H. Wang, *J. Cryst. Growth* **295**, 158 (2006).
- [47] C. Arnaboldi *et al.*, *J. Cryst. Growth* **312**, 2999 (2010).
- [48] C. Arnaboldi, C. Brofferio, C. Bucci, P. Gorla, G. Pessina and S. Pirro, *Nucl. Instrum. Meth. A* **554**, 300 (2005).
- [49] L. Cardani, L. Gironi, J. W. Beeman, I. Dafinei, Z. Ge, G. Pessina, S. Pirro and Y. Zhu, *J. Instrum.* **7**, P01020 (2012).
- [50] F. Alessandria *et al.*, *Astropart. Phys.* **35**, 839 (2012).
- [51] F. Alessandria *et al.*, *Astropart. Phys.* **45**, 13 (2013).
- [52] A. Alessandrello *et al.*, Proc. 4th Int. Workshop on Low Temp. Det. for Neutrinos and Dark Matter, 99 (1991).
- [53] A. Alessandrello, D. V. Camin, E. Fiorini, A. Giuliani and G. Pessina, *Nucl. Instrum. Meth. A* **264**, 93 (1988).
- [54] A. Alessandrello, C. Brofferio, D. V. Camin, O. Cremonesi, E. Fiorini, A. Giuliani and G. Pessina, *Phys. Lett. B* **247**, 442 (1990).
- [55] A. Alessandrello, C. Brofferio, D. V. Camin, O. Cremonesi, E. Fiorini, A. Giuliani and G. Pessina, *Physica B* **165-166**, 1 (1990).
- [56] A. Alessandrello *et al.*, *Nucl. Instrum. Meth. A* **315**, 263 (1992).
- [57] A. Giuliani *et al.*, Proc. Joint Int. Lepton Photon Symposium at High Energies (15th) and European Phys. Soc. Conf. on High-energy Phys., 670 (1991).
- [58] A. Alessandrello, C. Brofferio, D. V. Camin, O. Cremonesi, E. Fiorini, A. Giuliani, G. Pessina and E. Previtali, Proc. 3rd Int. Workshop on Low Temp. Det. for Neutrinos and Dark Matter, 253 (1989).
- [59] A. Alessandrello *et al.*, *Nucl. Phys. B* (Proc. Suppl.) **28 A**, 229 (1992).
- [60] A. Alessandrello *et al.*, *IEEE Trans. Nucl. Sci.* **39**, 610 (1992).
- [61] A. Alessandrello *et al.*, Proc. SPIE, Gamma-Ray Detectors **1734**, 177 (1992).
- [62] A. Alessandrello *et al.*, *Nucl. Instrum. Meth. B* **142**, 163 (1998).
- [63] A. Alessandrello *et al.*, *Nucl. Phys. B* (Proc. Suppl.) **31**, 83 (1993).
- [64] A. Alessandrello *et al.*, *Phys. Lett. B* **335**, 519 (1994).
- [65] A. Giuliani *et al.*, Proc. 27th Int. Conf. on High-energy Phys., 943 (1994).
- [66] A. Alessandrello *et al.*, *Nucl. Phys. B* (Proc. Suppl.) **48**, 238 (1996).
- [67] A. Alessandrello *et al.*, *Nucl. Instrum. Meth. A* **360**, 363 (1995).
- [68] S. Pirro *et al.*, *Nucl. Instrum. Meth. A* **444**, 331 (2000).
- [69] S. Pirro, *Nucl. Instrum. Meth. A* **559**, 672 (2006).
- [70] A. Alessandrello *et al.*, *Nucl. Instrum. Meth. A* **370**, 269 (1996).
- [71] C. Arnaboldi *et al.*, *Phys. Lett. B* **557**, 167 (2003).
- [72] M. Pedretti, (2004), [Ph.D. thesis, Università dell'Insubria].
- [73] A. Alessandrello *et al.*, *Phys. Lett. B* **486**, 13 (2000).
- [74] A. Alessandrello *et al.*, *Nucl. Instrum. Meth. A* **444**, 111 (2000).
- [75] G. Pessina, *Nucl. Instrum. Meth. A* **444**, 132 (2000).
- [76] A. Alessandrello *et al.*, *Phys. Lett. B* **433**, 156 (1998).
- [77] S. Capelli, (2005), [Ph.D. thesis, Università di Milano].
- [78] C. Alduino *et al.* (CUORE Collaboration), *J. Instrum.* **11**, P07009 (2016).
- [79] Cuoricino detector shielded by courtesy of S. Pirro.
- [80] E. Fiorini, *Phys. Rep.* **307**, 309 (1998).
- [81] A. Alessandrello *et al.*, *Nucl. Instrum. Meth. A* **440**, 397 (2000).
- [82] C. Arnaboldi, C. Bucci, S. Capelli, P. Gorla, E. Guardincerri, A. Nucciotti, G. Pessina, S. Pirro and M. Sisti, *IEEE Trans. Nucl. Sci.* **52**, 1630 (2005).
- [83] C. Arnaboldi *et al.*, *Nucl. Instrum. Meth. A* **520**, 578 (2004).
- [84] C. Arnaboldi *et al.* (Cuoricino Collaboration), *Phys. Rev. C* **78**, 035502 (2008).
- [85] E. Andreotti *et al.*, *Astropart. Phys.* **34**, 822 (2011).
- [86] S. Sangiorgio, (2006), [Ph.D. thesis, Università dell'Insubria].
- [87] A. Giachero, (2008), [Ph.D. thesis, Università di Genova].
- [88] C. Rusconi, (2011), [Ph.D. thesis, Università dell'Insubria].
- [89] P. Gorla, (2006), [Ph.D. thesis, Università di Milano-Bicocca].
- [90] L. Foggetta, A. Giuliani, C. Nones, M. Pedretti, C. Salvioni and S. Sangiorgio, *Astropart. Phys.* **34**, 809 (2011).
- [91] M. Wójcik and G. Zuzel, *AIP Conf. Proc.* **897**, 53 (2007).
- [92] E. Buccheri, M. Capodiferro, S. Morganti, F. Orio, A. Pelosi and V. Pettinacci, *Nucl. Instrum. Meth. A* **768**, 130 (2014).
- [93] M. Clemenza, C. Maiano, L. Pattavina and E. Previtali, *Eur. Phys. J. C* **71**, 1805 (2011).
- [94] E. Andreotti *et al.*, *J. Instrum.* **4**, P09003 (2009).
- [95] C. Brofferio, L. Canonica, A. Giachero, C. Gotti, M. Maino and G. Pessina, *Nucl. Instrum. Meth. A* **718**, 211 (2013).
- [96] D. R. Artusa *et al.* (CUORE Collaboration), *Adv. High Energy Phys.* **2015**, 879871 (2015).
- [97] C. Alduino *et al.* (CUORE Collaboration), *Phys. Rev. C* **93**, 045503 (2016).
- [98] C. Alduino *et al.* (CUORE Collaboration), *Eur. Phys. J. C* **77**, 543 (2017).
- [99] S. Dell'Oro, (2017), [Ph.D. thesis, INFN - Gran Sasso Science Institute].
- [100] G. Benato *et al.*, (2017), arXiv:1711.07936 [physics.ins-det].
- [101] A. D'Addabbo, C. Bucci, L. Canonica, S. Di Domizio, P. Gorla, L. Marini, A. Nucciotti, I. Nutini, C. Rusconi and B. Welliver, (2017), arXiv:1712.02753 [physics.ins-det].
- [102] F. Alessandria *et al.*, *Nucl. Instrum. Meth. A* **727**, 65 (2013).
- [103] F. Alessandria *et al.*, The CUORE cryostat: a 10 mK infrastructure for large bolometric arrays (2018), [Paper in preparation].
- [104] J. S. Cushman *et al.*, *Nucl. Instrum. Meth. A* **844**, 32 (2017).
- [105] O. Cremonesi, (2017), [To appear in the proceedings of TAUP 2017].
- [106] C. Alduino *et al.* (CUORE Collaboration), (2017), arXiv:1710.07988 [nucl-ex].
- [107] K. Alfonso *et al.* (CUORE Collaboration), *Phys. Rev. Lett.* **115**, 102502 (2015).
- [108] T. Kirsten, H. Richter and E. Jessberger, *Phys. Rev. Lett.* **50**, 474 (1983).

- [109] A. Alessandrello *et al.*, *Phys. Lett. B* **285**, 176 (1992).
- [110] A. Gando *et al.* (KamLAND-Zen Collaboration), *Phys. Rev. Lett.* **117**, 082503 (2016).
- [111] L. Pandola, (2017), [To appear in the proceedings of TAUP 2017].
- [112] C. Alduino *et al.* (CUORE Collaboration), *Eur. Phys. J. C* **77**, 532 (2017).
- [113] S. Dell’Oro, M. Marcocci, S. and Viel and F. Vissani, *Adv. High Energy Phys.* **2016**, 2162659 (2016).
- [114] J. Kotila and F. Iachello, *Phys. Rev. C* **85**, 034316 (2012).
- [115] J. Barea, J. Kotila and F. Iachello, *Phys. Rev. C* **91**, 034304 (2015).
- [116] F. Šimkovic, V. Rodin, A. Faessler and P. Vogel, *Phys. Rev. C* **87**, 045501 (2013).
- [117] A. Faessler, G. L. Fogli, E. Lisi, V. Rodin, A. M. Rotunno and F. Šimkovic, *J. Phys. G* **35**, 075104 (2008).
- [118] J. Barea, J. Kotila and F. Iachello, *Phys. Rev. C* **87**, 014315 (2013).
- [119] R. G. H. Robertson, *Mod. Phys. Lett. A* **28**, 1350021 (2013).
- [120] S. Dell’Oro, S. Marcocci and F. Vissani, *Phys. Rev. D* **90**, 033005 (2014).
- [121] J. Engel and J. Menéndez, *Rep. Prog. Phys.* **80**, 046301 (2017).
- [122] E. Lisi, A. Rotunno and F. Šimkovic, *Phys. Rev. D* **92**, 093004 (2015).
- [123] J. Suhonen, *Phys. Rev. C* **96**, 055501 (2017).
- [124] D. R. Artusa *et al.* (CUORE Collaboration), *Eur. Phys. J. C* **74**, 3096 (2014).
- [125] D. R. Artusa *et al.*, *Phys. Lett. B* **767**, 321 (2017).
- [126] M. Vignati, (2010), [Ph.D. thesis, Università di Roma La Sapienza].
- [127] D. Santone, (2017), [Ph.D. thesis, Università dell’Aquila].
- [128] A. F. Barghouty *et al.*, *Nucl. Instrum. Meth. B* **295**, 16 (2013).
- [129] N. Casali *et al.*, *Eur. Phys. J. C* **75**, 12 (2015).
- [130] D. R. Artusa *et al.*, *Eur. Phys. J. C* **76**, 364 (2016).
- [131] G. B. Kim *et al.*, *Adv. High Energy Phys.* **2015**, 817530 (2015).
- [132] E. Armengaud *et al.*, *Eur. Phys. J. C* **77**, 785 (2017).
- [133] I. Dafinei, M. Diemoz, E. Longo, A. Peter and I. Foldvari, *Nucl. Instrum. Meth. A* **554**, 195 (2005).
- [134] I. Dafinei, C. Dujardin, E. Longo and M. Vignati, *Phys. Status Solidi A* **204**, 1567 (2007).
- [135] T. Tabarelli de Fatis, *Eur. Phys. J. C* **65**, 359 (2010).
- [136] F. Bellini *et al.*, *J. Instrum.* **9**, P10014 (2014).
- [137] J. W. Beeman *et al.*, *Astropart. Phys.* **35**, 558 (2012).
- [138] F. Bellini, N. Casali, I. Dafinei, M. Marafini, S. Morgananti, F. Orio, D. Pinci, M. Vignati and C. Voena, *J. Instrum.* **7**, P11014 (2012).
- [139] G. Wang *et al.* (CUPID Collaboration), (2015), arXiv:1504.03599 [physics.ins-det].
- [140] G. Wang *et al.* (CUPID Collaboration), (2015), arXiv:1504.03612 [physics.ins-det].
- [141] E. S. Battistelli *et al.*, *Eur. Phys. J. C* **75**, 353 (2015).
- [142] F. Bellini *et al.*, *Appl. Phys. Lett.* **110**, 033504 (2017).
- [143] K. Schäffner *et al.*, *Astropart. Phys.* **69**, 30 (2015).
- [144] M. Willers *et al.*, *J. Instrum.* **10**, P03003 (2015).
- [145] L. Pattavina *et al.*, *J. Low. Temp. Phys.* **184**, 286 (2016).
- [146] M. Biassoni *et al.*, *Eur. Phys. J. C* **75**, 480 (2015).
- [147] L. Gironi *et al.*, *Phys. Rev. C* **94**, 054608 (2016).
- [148] L. Bergé *et al.*, (2017), arXiv:1710.03459 [physics.ins-det].
- [149] C. Nones, L. Bergé, L. Dumoulin, S. Marnieros and E. Olivieri, *J. Low. Temp. Phys.* **167**, 1029 (2012).
- [150] L. Canonica, M. Biassoni, C. Brofferio, C. Bucci, S. Calvano, M. L. Di Vacri, J. Goett, P. Gorla, M. Pavan and M. Yeh, *Nucl. Instrum. Meth. A* **A732**, 286 (2013).
- [151] F. Capozzi, E. Lisi, A. Marrone, D. Montanino and A. Palazzo, *Nucl. Phys. B* **908**, 218 (2016).
- [152] R. Arnold *et al.* (NEMO-3 Collaboration), *Phys. Rev. D* **92**, 072011 (2015).
- [153] J. Hyvarinen and J. Suhonen, *Phys. Rev. C* **91**, 024613 (2015).
- [154] F. Vissani, *J. High Energy Phys.* **9906**, 022 (1999).
- [155] C. Bucci, What Next -  $0\nu\beta\beta$  (2014), [Public seminar at LNGS].
- [156] M. Agostini *et al.* (GERDA Collaboration), *Nature* **544**, 5 (2017).
- [157] H. London, Proc. 2nd Int. Conf. on Low Temp. Phys., 157 (1951).
- [158] H. London, G. R. Clarke and E. Mendoza, *Phys. Rev.* **128**, 1992 (1962).
- [159] P. Das, R. De Bruyn Ouboter and K. W. Taconis, Proc. 9th Int. Conf. on Low Temp. Phys., 1253 (1965).
- [160] G. Frossati, *J. Phys. Colloques* **39**, C6–1578 (1978).
- [161] D. J. Cousins, S. N. Fisher, A. M. Guénault, R. P. Haley, I. E. Miller, G. R. Pickett, G. N. Plenderleith, P. Skyba, P. Y. A. Thibault and M. G. Ward, *J. Low Temp. Phys.* **114**, 547 (1999).
- [162] F. Pobell, *Matter and Methods at Low Temperatures* (Springer, 2007).
- [163] W. E. Gifford and R. C. Longsworth, *Trans. ASME J. Eng. Ind.* **3**, 264 (1964).